Hindawi Publishing Corporation
Advances in Condensed Matter Physics
Volume 2011, Article ID 727958, 22 pages
doi:10.1155/2011/727958

Review Article

Experimental Progress towards Probing the Ground State of an Electron-Hole Bilayer by Low-Temperature Transport

K. Das Gupta,[1] A. F. Croxall,[1] J. Waldie,[1] C. A. Nicoll,[1] H. E. Beere,[1] I. Farrer,[1] D. A. Ritchie,[1] and M. Pepper[1,2]

[1] *Cavendish Laboratory, University of Cambridge, J.J. Thomson Avenue, Cambridge CB3 0HE, UK*
[2] *Department of Electronic and Electrical Engineering, University College, London WC1E7JE, UK*

Correspondence should be addressed to K. Das Gupta, kd241@cam.ac.uk

Received 27 May 2010; Accepted 27 October 2010

Academic Editor: Milica Milovanovic

Recently, it has been possible to design independently contacted electron-hole bilayers (EHBLs) with carrier densities $< 5\times10^{10}$ cm^2 in each layer and a separation of 10–20 nm in a GaAs/AlGaAs system. In these EHBLs, the interlayer interaction can be stronger than the intralayer interactions. Theoretical works have indicated the possibility of a very rich phase diagram in EHBLs consisting of excitonic superfluid phases, charge density waves, and Wigner crystals. Experiments have revealed that the Coulomb drag on the hole layer shows strong nonmonotonic deviations from a $\sim T^2$ behaviour expected for Fermi-liquids at low temperatures. Simultaneously, an unexpected insulating behaviour in the single-layer resistances (at a highly "metallic" regime with $k_F l > 500$) also appears in both layers despite electron mobilities of above $\sim 10^6$cm^{2}V^{-1}s^{-1} and hole mobilities over $\sim 10^5$cm^{2}V^{-1}s^{-1}. Experimental data also indicates that the point of equal densities ($n = p$) is not special.

1. Introduction

Bringing two layers of 2-dimensional electron gases (2DEG) or a 2-dimensional hole gases (2DHG) in close proximity opens up possibilities that do not exist when the layers are very far apart. We give a simple example to show why interaction-driven phases can arise more readily in bilayers. Let us recall that the ratio of the kinetic energy of a system of electrons and their potential energies due to mutual Coulomb interaction is measured by the parameter $r_s = E_{ee}/E_f$ (where $E_{ee} = e^2\sqrt{(\pi N)}/4\pi\epsilon_0\epsilon_r$ and $E_f = \pi\hbar^2 N/m^*$ in 2-dimensions, with N electrons per unit area). The ratio is not material independent; it depends on parameters like the relative dielectric constant ϵ_r and the band effective mass m^* of the material. Confining a large number of particles in a small area makes the interparticle spacing small and hence the Coulomb repulsion large, but the kinetic energy of the particles increases even faster—making r_s smaller. This somewhat counterintuitive fact is a straightforward consequence of Fermi statistics and is true in all dimensions. Consider now two parallel layers of electrons or holes with 10^{11} cm^{-2} electrons in each—which is a typical density in many experiments based on GaAs-AlGaAs heterostructures. If they are now brought closer to each other, the particles in one layer not only interact with others in the same layer but also with those in the other layer. The interparticle spacing in the same layer stays fixed and is about 30 nm. It is now possible to make the distance between the two layers about 10 nm with negligible tunneling taking place. 10 nm is approximately the excitonic Bohr radius in gallium arsenide (GaAs) and is an important length scale. We thus get an electron to "see" another electron (or hole) only 10 nm away, without paying the kinetic (Fermi) energy cost, because the two layers continue to be two separate Fermi systems. To get the same average interparticle separation (i.e., 10 nm) within a layer, a 9-fold increase in density (and hence Fermi energy) would have been necessary. As a consequence interaction-driven phases may be expected to occur more readily in bilayers. The case of the electron-hole bilayer may have some remarkable possibilities—particularly if we can make the interlayer attractive interaction stronger than the intralayer repulsive interactions. This will require a bilayer system

where the particles have low enough densities, such that the intralayer separation between the particles is larger (or of the same order) than the interlayer distance. In practice, this implies that if the layer densities are about 10^{11} cm^{-2}, then the interlayer distance would have to be about 10–20 nm.

First, because of the attractive interaction between the electrons and holes, bound pairs may form. Indeed, bound pairs of electrons and holes (excitons) are well known in bulk semiconductors. However, there is a crucial difference here. In bulk, the lifetime of the excitons can rarely exceed a few nanoseconds, because of radiative decay. The idea that spatially separating electrons and holes could be a fruitful way of obtaining large exciton lifetimes and possible "bosonic" phases was first proposed in 1975 [1, 2]. Although this is a very exciting possibility, there can be many legitimate questions about how stable such a condensate would be, whether in 2-dimensions one can get a long-range coherence at all, and so forth. It is not known how to measure the momentum distribution (characteristic of a condensate) of a bunch of particles by transport—but there is another class of transport-based experiments [3–5] that can turn out to be very useful; these are measurements of the transresistivity of the bilayer, which can be directly related to the interlayer scattering rate and may also provide indications of a condensate phase [6–8]. Passing current in both layers in an opposite sense (counterflow) is predicted to couple to the excitons and is expected to be dissipationless for a superfluid [9]. A large increase in the drag resistivity is also expected [6, 10]. Noise measurements, response to parallel magnetic field, and Josephson junction-like behaviour across a weak link are also anticipated [9, 10].

The first proposals [1, 2] relied on n-semiconductor-insulator-p-semiconductor structures to achieve this. However, only with the rapid improvements in GaAs/AlGaAs, heterostructure technology in the 1980s and subsequent development of closely spaced double quantum-well structures in the 1990s led to the first realistic possibilities of making such a system. In 2D, the relationship between the critical density and the superfluid transition temperature (T_{KT}) is expected to be given by the Kosterlitz-Thouless condition

$$n_{\mathrm{ex}} \sim \frac{1}{\hbar^2} m^*_{\mathrm{ex}} k_B T_{\mathrm{KT}}, \tag{1}$$

where n_{ex} is the exciton density and m^*_{ex} is the effective mass of the exciton [2]. In semiconductors, the small effective mass of an exciton ($\sim 0.2m_e$) means that the transition temperature is anticipated to be much higher than that required for atomic BEC. The possibility of excitonic BEC in EHBLs has been reviewed by Littlewood and Zhu [11].

The second possibility is somewhat less intuitive. It involves the densities of the two layers developing a spontaneous periodic modulation. Loosely speaking, it would remind one of a homogeneous liquid freezing to a solid which has a crystal structure. Such spontaneous ordering may be characterized by the divergence of the relevant susceptibility function at a particular wavevector. Simple theories describing the susceptibility of a 2DEG (Lindhard response function) would predict that the susceptibility remains nearly constant till $q = 2k_F$ (where k_F is the Fermi wavevector) and drops rapidly to zero after that. This indeed is the correct behaviour at long wavelengths, but it leads to certain unphysical results at short-length scales. A theory of susceptibility also leads to predictions for the two particle probability distribution $g(r)$. This is not hard to see. Susceptibility is the density-density response function of a system, which by the fluctuation-dissipation theorem is directly related to the density-density fluctuation or the structure factor. The structure factor, in turn is the Fourier transform of the two particle probability distribution. Among the well-known attempts [12–14] to get the physically reasonable (nonnegative) values of $g(r)$ at small distances is a self-consistent local-field theory of Singwi et al. This approach connects the charge susceptibility, structure factor, and the local-field corrections for the screened Coulomb potential. With the advent of double quantum well structures in the early 1990s, this was extended successfully to the bilayer [15–17]. A striking prediction of [17, 18] is that the electron-hole bilayer would be more susceptible to a charge density wave (CDW) formation at wavevectors much smaller than k_{F} than the electron-electron bilayer. The density-modulated phases are indicated by the divergence of one of the eigenvalues of the bilayer susceptibility matrix, but this does not require the divergence of the single-layer susceptibilities—which may still occur at much higher r_s. An excitonic state may be indicated by a divergence in the interlayer pair-correlation function $g_{12}(r)$ at $r = 0$; Liu et al. [18] had proposed that such a divergence would be preceded by a CDW.

How close do we want the two layers to be? If we want to make the interlayer interaction stronger than the intralayer interaction, then we need the interlayer distance (d) to be smaller than the intralayer separation (l) of the particles. Thus, for example, for $N = 10^{11}$ cm^{-2} in each layer, we would want $d \approx$ 10–20 nm. It is easy to see that the d/l ratio would be indicative of the relative strength of the interlayer and intralayer interactions. At the same time, it is important to ensure that the electron and mobilities are sufficiently high such that their behaviour is not predominantly dictated by localisation and inhomogeneity.

2. Making Real Bilayers

While remarkable possibilities were predicted for EHBLs, making them experimentally turned out to be difficult and challenging. In this section, we will try to see why the basic requirements for making transport measurements in EHBLs turned out to be difficult. Since the first attempt by Sivan et al. [19], there was a continued interest in these devices marked by the work of Kane et al. (1994) [20], Rubel et al. (1998) [21], Pohlt et al. (2002) [22], Keogh et al. (2005) [23], and Seamons et al. (2007) [24]. There are a few key requirements for working with bilayers:

(i) independent ohmic contacts to each layer,

(ii) gate voltage control of the densities of each layer,

(iii) very low leakage through the barrier separating the two layers.

2.1. Making Independent Ohmic Contacts. Achieving independent ohmic contact to each layer in an EHBL is considerably more difficult than in electron-electron or hole-hole bilayers. Let us first look at the basic idea behind independently contacting a 2x2DEG. Figure 1 shows how the ohmic contact, usually indium or a gold-germanium-nickel alloy, is deposited at selected places using standard photolithographic techniques. The subsequent annealing process causes the metal to diffuse into the semiconductor and pass through both wells. The contacts are not independent at this stage, since they pass through and contact both layers. To achieve independent contact to the bottom layer, the front gate (on the surface side) is biased negatively with respect to the ohmics such that only the upper electron gas is depleted. The gate raises the conduction band, creating a potential hill just below it. So, the left contact (as in Figure 1) contacts only the bottom 2DEG. If we now have a similar gate at the bottom of the sample, then a negative voltage on that gate would locally deplete the lower 2DEG, allowing us to contact only the top 2DEG (as shown on the right). The gates below the 2x2DEG must be aligned to the topside features of the device, correct to a few microns, to ensure that the lower 2DEG is selectively depleted.

There is also another practical point. The topgate is typically only a few hundred nanometers above the upper 2DEG, so a small voltage on that gate will have sufficient effect on the 2DEG. But the substrate (gallium arsenide) is itself about half a millimeter (500 microns) thick. So, a voltage on the backgate (irrespective of whether it is aligned or not), will have 1000 times less effect on the 2DEG. Therefore, the sample needs to be thinned to lower the biases required. It is practical to make the samples about 50 microns in thickness and still handle them. So, the voltages required would come down to about 50–100 volts, which is practical. This was done by Eisenstein et al. in 1990 [25]. Aligning the backgate with topside features is another crucial requirement. This in general requires a double-sided mask aligner. A process to achieve this with a single-side mask aligner and thinned substrates ($\approx 50\,\mu$m) was developed by the authors' group and has been described in detail in [26].

There are two possible ways of bringing the backgate almost as close to the quantum wells as the topgate so that the voltages required are comparable. One of these is based on the Focussed Ion Beam (FIB) technique. The second involves making the sample itself 1-2 microns thick by etching from the back, using an etch stop layer, using a technique named "Epoxy bond and stop etch" (EBASE) described by Weckwerth et al. [27].

If a conducting region could be grown (during MBE) only at places where we want the backgate (as in Figure 1), then this would be a nice way to selectively deplete the bottom 2DEG. Doped GaAs conducts because the dopants (Si) occupy some of the Ga lattice sites and contributes one electron to the conduction band. If certain regions are selectively subjected to a beam of heavy ions, then the regions become nonconducting. Large defect densities may be created which trap the electrons released by the donor atoms or the Si atoms may be displaced—in either

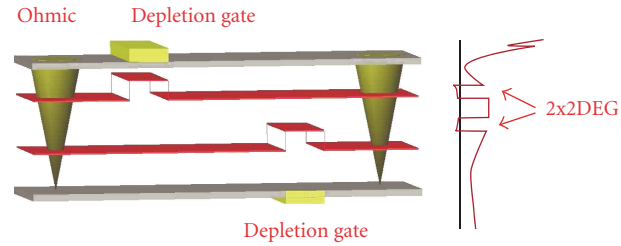

Figure 1: A schematic representation for independent ohmic contacts to a 2x2DEG. A similar method will work for a 2x2DHG as well. Notice that the 2DEG exists due to carriers from ionised dopants before the contacts are made. The sketch on the right hand side shows the rough profile of the bottom of the conduction band.

case, electrons from the donor atoms would not be able to populate the conduction band. Experimentally, this can be done by using a beam of Ga ions at 30 keV or so from a focussed ion gun. Ion doses like 10^{12}–$10^{13}\,\mathrm{cm}^{-2}$ would disrupt the lattice sufficiently and the n^+ layer would be rendered resistive (say $10^{14}\,\Omega$ at 1.5 K). The beam can be directed with high accuracy and write out a desired a pattern. The layers which make up the double quantum well (DQW) structures are grown after this stage. The entire patterning process and subsequent growth is done without removing the sample from the ultra high vacuum (UHV) environment, to prevent contamination. This is the basis of the focussed-ion-beam (FIB) method and has also been successfully used for making transport measurements on independently contacted DQW by Hill et al. [28] and Linfield et al. [29]. Notice that the area on which the active region of the sample will be located is actually not the beam damaged area—this still allows high 2DEG mobilities to be reached. A pertinent question at this stage is how to align the later photolithographic stages with the damaged/undamaged area pattern written out by the beam. Very high ion doses of $10^{17}\,\mathrm{cm}^2$ or so can be used to etch alignment marks away from the central region where the 2DEG forms. This level of beam damage makes the subsequent growth on those areas visibly different due to high concentration of defects. The later stages can thus be aligned with the buried backgates.

3. The Electron-Hole Bilayer

Is it possible to extend a modulation doping-based method of making 2x2DEGs and 2x2DHGs to make an electron-hole bilayer (EHBL)? The answer is that it is possible only if we are satisfied with very large layer separations $d > 100$ nm [21]. At that distance, the interlayer Coulomb interaction would not be dominant. Consider a situation where we try to create two modulation-doped gases, (one 2DEG and one 2DHG) in close proximity, say 10–20 nm. The Fermi level must come above the conduction band for a 2DEG to form; similarly, it must fall slightly below the valence band for a hole gas to form. Now, the top of the valence band and the bottom of the conduction band are separated by 1.5 V, which is the bandgap of GaAs. Thus, if a 2DEG and a 2DHG exist at the same electrochemical potential, then the bands must have a

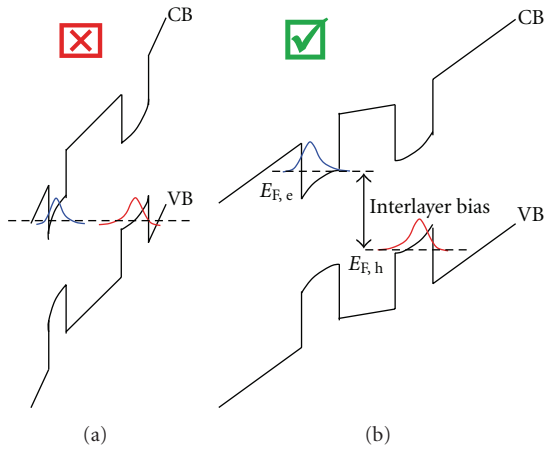

FIGURE 2: The band bending shown on (a) is not possible to achieve in GaAs for a closely spaced EHBL. The electric field in the barrier would be too high to sustain or even obtain self-consistently by modulation doping alone. One has to resort to making the electrochemical potential discontinuous (as shown on (b)). This was already understood in 1992.

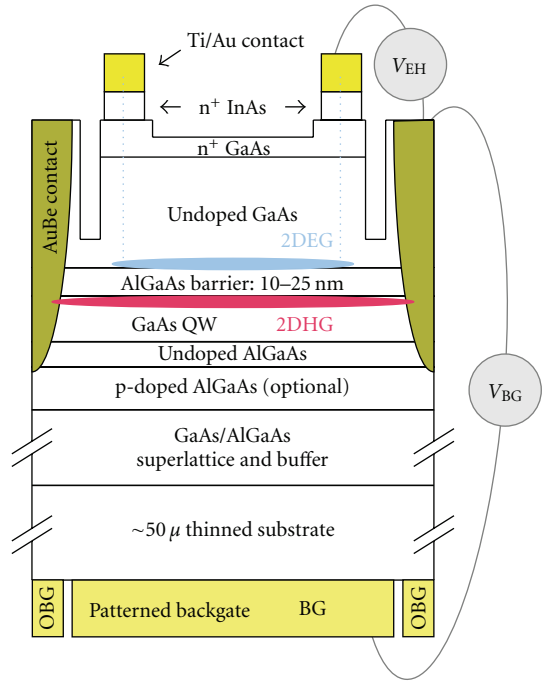

FIGURE 3: The schematic representation of the EHBL developed in the authors' group. Note that two voltage biases are in general needed for operating the device. However, the outer backgate below the ohmic contacts (V_{obg}) to the holes is often biased differently from the backgate in the central region (V_{bg}).

very large slope in the region between the two layers. This implies an electric field of $\sim 10^8$ V/m, which is too high to sustain. The structure would simply collapse. See Figure 2. As an aside, the bandgap of Silicon is about 1.1 V, so the required field would be slightly less. In fact, recently, two groups have succeeded in making EHBLs in Si [29, 30], where the electrons and holes stay at the same chemical potential. If at some point independent contact to bilayer graphene is made, then it would be very interesting from the point of view of an EHBL, because the bandgap of graphene is zero. However, in the GaAs-AlGaAs system, the only way around would be to make the electrochemical potential itself discontinuous. This means that we need to connect a battery from outside between the two layers which would allow the two gases to exist without requiring a huge band slope.

Notice that even before we made independent contacts, it was possible to create a a 2x2DEG. In the case of the EHBL, the contact must exist before the electron and hole gases can be formed. This also calls for the barrier between the two layers to be exceptionally uniform and robust. At the heart of most bilayer devices (particularly EHBLs) is this barrier that separates the two layers. For closely spaced (10 nm) bilayers, a single growth defect in an area $\sim 100\,\mu\text{m} \times 100\,\mu\text{m}$ will cause everything to be dominated by catastrophic leakage and not bilayer physics! This extremely stringent requirement on the uniformity of the barrier layer is equivalent to placing two sheets of cloth over an area of a football field while maintaining a uniform vertical distance of 1 cm between them throughout (if we scale all the lengths by a factor of a million). These issues were quite well appreciated, and the first EHBL device was made in early 1990s by Sivan et al. But this device had limited range of operation as far as the density and temperatures (above 9 K only) were concerned [19]. Only in last 3-4 years, it has been possible to make EHBLs where transport can be measured down to millikelvin temperatures, densities can be tuned over a large range, and the interlayer interaction can be made stronger than the intralayer interaction due to d/l values reaching below 1.

3.1. Recent Designs Of Electron-Hole Bilayers. The discussion in the previous section makes it clear that for an EHBL to exist in a GaAs/AlGaAs structure, the electron and hole layers must be held at different electrochemical potentials, and hence each layer must act as a gate for the other. Thus, a combination of modulation doping and biasing can be used to achieve a stable electron and hole population. Here, we describe the device fabricated by the authors' group [23, 26, 31]. We begin with an inverted hole gas created with a very low level of doping so that it can be backgated. A high level of doping would prevent the backgate from acting on the 2DHG. Exactly what level of doping would stop a gate from working is an interesting and somewhat difficult question [26]. Making contact to this hole layer is not difficult. This is usually done by depositing some gold-beryllium alloy and annealing the metal to make it diffuse into the semiconductor. See Figure 3 for a device schematic representation and Figure 4 for a self-consistent band structure.

Now, using the hole layer as a gate, we can induce an electron layer on the other side of the AlGaAs barrier (see Figure 4). Electrons start accumulating soon after the bias reaches the bandgap, provided there is some n-type ohmic contact to the electron layer, from where carriers can be pulled into the heterointerface. Fabricating such a device

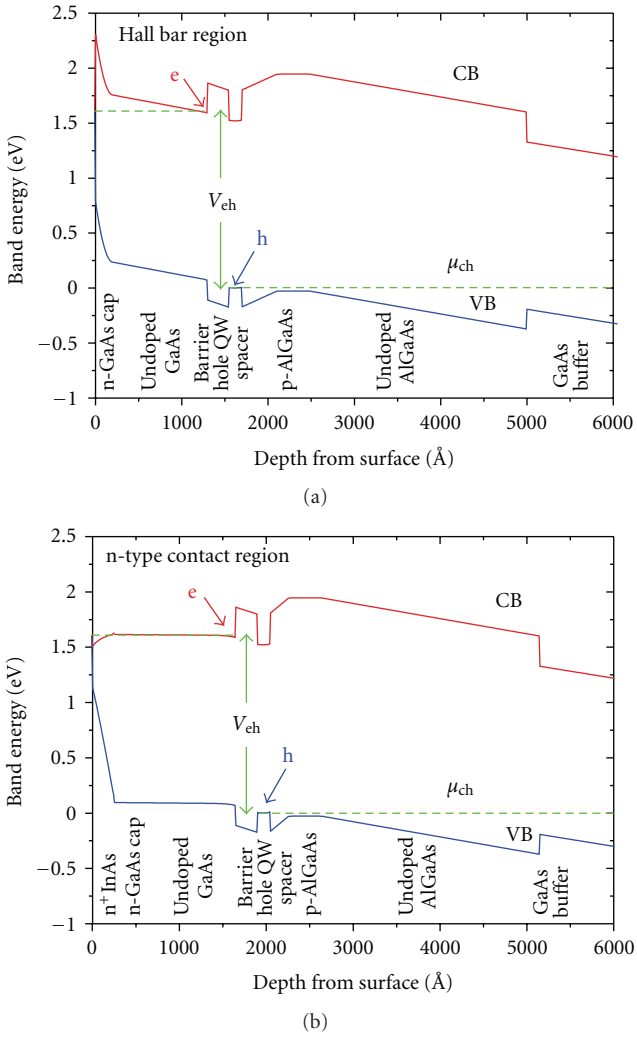

FIGURE 4: Self-consistent band structure calculations (a) of the Hall-bar region and (b) the n-type contact region of the device developed in the authors' group.

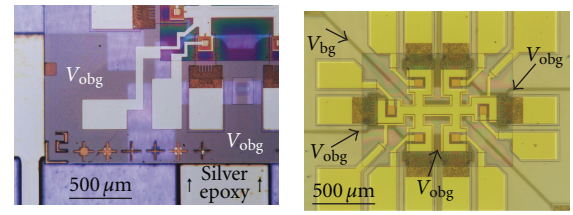

FIGURE 5: Composite IR and visible photographs (a) Backgated sample mounted on host substrate with etched channels indicated to contact backgate with silver epoxy. (b) Thinned sample with outer backgates (V_{obg}) and central backgate (V_{bg}) visible.

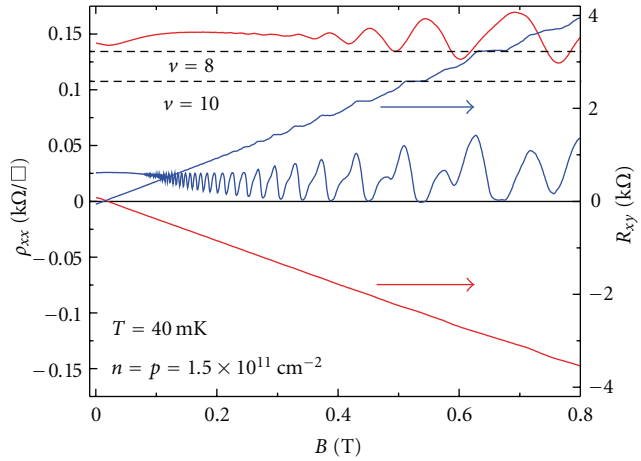

FIGURE 6: 2DEG and 2DHG in an EHBL made by the method described in [23, 26, 31] (Cavendish Laboratory).

requires some new thinking. An usual diffused ohmic would not work, because it would penetrate the barrier and reach the hole layer as well. The method would work only if we can find a "nonspiking" ohmic. Fortunately, there is a way. A heavily doped capping layer of InAs (8×10^{18} cm^{-3} Si) is used to pin the Fermi-level *above* the conduction band at the surface of the wafer. A selective etchant (conc. HCl) is used to remove the InAs from all regions except from where the n-type contacts are to be formed. Any metal which adheres well to this surface (e.g., Ti/Au) can be used to inject electrons into the InAs layer at any infinitesimal bias. A "Schottky barrier", normally observed at a metal semiconductor interface, is not formed in this case. Though calculations indicate a small barrier at the interface of the InAs and n-GaAs, unless the composition is smoothly graded, experimentally, we have not found evidence of such a barrier. A flatband condition (see Figure 4) is maintained in the region below the contacts down to the 2DEG, forming a completely "nonspiking" contact to the electron QW induced above the barrier. However, the 2DEG must not be allowed to extend out to the spiking p-type contacts, else independent contact between the two layers would be lost. A carefully controlled isolation etch is introduced between each pair of n and p contacts. The etch removes sufficient GaAs to depopulate the upper electron QW, but does not interrupt the lower hole QW. Fully independent contacts are thus achieved without the need of any depletion gates, focussed ion beam, ion implantation, or shadow masking during MBE growth. All the necessary processing can be done with standard photolithographic techniques.

A composite IR and visible photo is shown in Figure 5(b) of a finished backgated device. The three independently controllable backgates are shown ($2 \times V_{obg}$ are tied together and V_{bg}). Each backgate is contacted at each end so that its continuity can be verified.

Figure 6 shows that the electron (blue) and hole (red) layers behave as 2-dimensional layers as expected.

The crucial point is that there must be independent contacts existing to both the electron and hole layers so that we can apply a voltage bias between them to get both layers to form. Another way was shown by Seamons et al. [24]. This design relies on two back-to-back field-effect transistors (FETs), one of which is an n-channel device, and the other

is p-channel. Under such circumstances, the gate of the FET needs a small overlap with the ohmic contact to ensure that there is continuous path from the contact to the channel which has the carriers. The device is in reality less than a micron thick and has to be supported on a substrate using a method described by Weckwerth et al. [27].

3.2. The $\nu = 1/2 + 1/2$ QHE Bilayer. In closely spaced 2x2DEGs and 2x2DHGs, excitonic BEC is believed to occur in large magnetic fields in the quantum Hall regime and to be observable with transport. When both layers are in the $\nu = 1/2$ state, the half-filled Landau levels may be considered to be half full of electrons and half full of holes [32]. Striking experiments in bilayer electrons by Kellogg et al. [33], Tiemann et al. [34] and in bilayer holes by Tutuc et al. [35] reveal almost dissipationless counterflow transport and vanishing counterflow Hall resistance. While in some ways these systems emulate exciton superfluidity in an EHBL (for zero magnetic field), there does exist a vacuum of Landau levels and the screening will be very different in magnetic fields. The relation between the physics in the $\nu = 1/2 + 1/2$ and the EHBL would doubtlessly be a very interesting area in near future—however, for the purposes of this paper, we have not addressed this question.

4. The Coulomb Drag Experiment

The ability to make independent contacts to bilayers makes some new transport measurements possible. These go by names like Coulomb drag, counterflow, parallel flow transport, and so forth. and can give us some information that single-layer measurements cannot. The basic importance of the drag measurement lies in the fact that it probes the interlayer scattering rate directly. The measurement involves sending a known current through one layer (I_{drive}) and measuring the open circuit voltage developed in the other layer as a result (V_{drag}). In the linear response regime, we can define a "drag resistance" $\rho_{\text{drag}} = V_{\text{drag}}/I_{\text{drive}}$, in analogy with normal resistance. In general, this has a strong temperature dependence. The electrons in one layer can see the Coulomb potential due to the electrons (or holes) in the other layer. Of course, this potential is not the bare Coulomb potential, but it would be the "screened" potential. The net result of this scattering is that the electrons in the drive layer try to impart a little bit of the momentum they have to the electrons in the other layer. This means that if we closed the circuit in the "drag" layer, a small current would actually flow, which has got nothing to do with leakage. This is very much like viscous drag between layers of a fluid. Usually, we prevent any current from flowing in the "drag" layer. So, a small pile up of charge occurs in one end of the layer which results in a voltage appearing across the "dragged" layer. This is the voltage we measure. The interesting (and useful) point is that the magnitude of this voltage is directly proportional to the scattering rate between the particles in different layers. As in any quantum mechanical calculation, the scattering rate is a product of a "matrix element" and another factor that gives the density of available states or the phase space" factor. The scattering rate between two electron gases was first measured by Gramilla et al. in 1991 [36].

In reality, one almost always uses low-frequency (few Hz) alternating current for these measurements, the measured voltage thus has an in-phase and an out-of-phase component. It can be shown that the out of phase component is proportional to the single-layer resistance and the measuring frequency.

4.1. Boltzmann Transport Analysis of the Drag Measurement. This problem has been quite extensively analysed by several authors in the context of 2x2DEGs (or 2x2DHGs) [5, 37–40] and for EHBLs as well [16, 41], using the linearized Boltzmann transport equation. Linearization is done in the way the Fermi distribution in the drive layer is assumed to change due to the current flow. Here, we quote the final result and point out a few important relevant features. Summing over all momentum exchange (q) between particles in the driven layer (layer 2) and dragged layer (layer 1), one gets [5]

$$\rho_{\text{drag}} = \frac{\hbar^3}{8\pi^2 e^2 kT n_1 n_2} \int d\omega \int \frac{d\mathbf{q}}{(2\pi)^2} W(1,2 \longrightarrow 1',2') \times \frac{q^3}{\sinh^2(\hbar\omega/2kT)} \operatorname{Im}\left(\chi_1^0(\mathbf{q},\omega)\right) \operatorname{Im}\left(\chi_2^0(\mathbf{q},\omega)\right). \tag{2}$$

Here, $W(1,2 \rightarrow 1',2')$ denotes the probability of the elastic scattering in which the momentum of a particle changes by q. χ_1^0 and χ_2^0 denote the noninteracting susceptibilities of the layers. n_1 and n_2 denote the carrier densities. Equation (2) is applicable to 2x2DEGs, 2x2DHGs, and EHBLs. The ratio of drag resistivity to single-layer resistivity is usually a small number, even for high-mobility double quantum well structures, around $T \sim 1K$, $\rho_{\text{drag}}/\rho_{\text{singlelayer}} \sim 10^{-2}$ or so at most.

Note that individual layer mobilities ($\mu = e\tau/m^*$, where τ is the intralayer relaxation time) do not occur in the expression. This is crucial and stems from the fact that while ordinary resistance is a measure of momentum lost to to all possible channels, the drag resistance is actually a direct measure of the momentum transferred to a single channel only.

Second, at small ω, $\operatorname{Im}(\chi(q,\omega)) \propto \omega$. This is useful at low temperatures, because as the frequency increases a little, the sinh factor in the denominator would start becoming large. Thus, it is easy to estimate the low T behaviour. We do not expect $W(1,2 \rightarrow 1',2')$ to have a strong temperature dependence, because the dielectric screening function does not have strong T dependence at small T. Substituting $\hbar\omega/kT = x$, then the dominant T dependence is easy to extract. We make a very robust prediction that measured drag (interlayer scattering rate) will be approximately $\propto T^2$, and go zero as $T \rightarrow 0$, due to the nature of the Fermi distribution function alone, independent of many details. It can be shown that for "weak coupling" (i.e., high density) at $T/T_{\text{F}} \ll 1$, and for a peak-to-peak separation of the two wavefunctions, d, one gets [5]

$$\rho_{\text{drag}} \propto \frac{T^2}{d^4 (n_1 n_2)^{3/2}}. \tag{3}$$

This prediction is well verified for 2x2DEGs and 2x2DHGs.

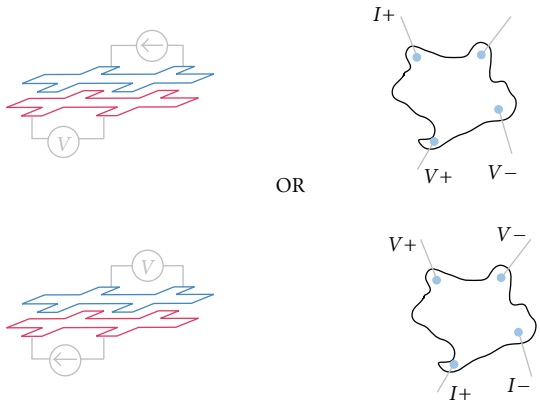

Figure 7: Schematic representation for the Coulomb drag measurement—notice that the measurement can be made in two ways. We may not look into the internal details of the sample and think of it as a "black box". Then, it just corresponds to changing the voltage and current probes, as shown on the right.

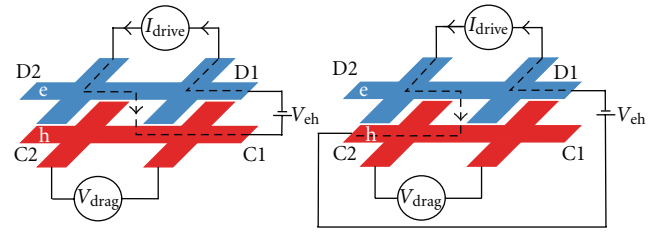

Figure 8: Diagram showing that a sign reversal of any error in drag due to excitation current leaking between layers is expected when biasing points (named C1, C2, D1, and D2) are altered, as direction in drag layer changed. A little bit of the drive current may be leaking into the other layer and flowing through a parallel path that includes part of the second layer. The resistive drop due to this would appear between the voltage probes. But it is possible to decide whether the measured voltage is due to this. If we change the point at which the second layer is grounded, the path of the leakage current would then be reversed causing the measured voltage to change. Thus, by shifting the point at which the "drag layer" is voltage referenced, we can verify if the measured voltage was due to leakage or not.

The coefficient of the T^2 term, however, requires a good model of dynamical screening of the interlayer Coulomb interaction. For the transition probability, we can use the Born approximation

$$W(1,2 \longrightarrow 1',2') = \frac{2\pi}{\hbar} \left| M_{1,2,\,1',2'}(q) \right|^2. \tag{4}$$

Here, M denotes the matrix element for a transition from state $(1,2)$ to a state $(1',2')$ The transitions are caused by the screened Coulomb potential of a particle in layer 1, as seen by another particle in layer 2. Thus, the measured drag gives us a very direct experimental handle on the generic physics of screening in a many body context. Here, we quote some of the relevant important results.

The *unscreened* Fourier component of the interaction potential due to a point charge in layer 1, as seen in the same layer ($\tilde{v}_{11}$), and in the other layer ($\tilde{v}_{12}$) can be written as

$$\begin{pmatrix} \tilde{v}_{11}(q) \\ \tilde{v}_{12}(q) \end{pmatrix} = \frac{e^2}{2\epsilon_0 \epsilon_r q} \begin{pmatrix} F_{11}(q) \\ F_{12}(q) \end{pmatrix}, \tag{5}$$

where the form factors $F_{ij}(q)$ takes into account the averaging of the potential over the subband charge distribution of each 2D gas. We can define $\tilde{v}_{21}$ and $\tilde{v}_{22}$ similarly

$$F_{ij}(q) = \int dz \int dz' \left| \psi_i(z) \right|^2 e^{-q|z-z'|} \left| \psi_j(z) \right|^2. \tag{6}$$

For infinitely narrow wells, the charge distributions approach delta functions. If these are separated by a distance d, then $F_{11}(q) = 1$ and $F_{12}(q) = e^{-qd}$.

The physically important screened components (v_{11},v_{12}) are obtained from the unscreened components ($\tilde{v}_{11}$,$\tilde{v}_{12}$) by summing the contributions of the original charge and the charges induced by the potential of the original charge. The connection is provided by the dielectric screening function $\epsilon(q,\omega)$, which is a 2×2 matrix in this case

$$\begin{pmatrix} v_{11} \\ v_{12} \end{pmatrix} = \epsilon(q,\omega)^{-1} \begin{pmatrix} \tilde{v}_{11} \\ \tilde{v}_{12} \end{pmatrix}. \tag{7}$$

The dielectric function can be written as

$$\epsilon(q,\omega) = \epsilon_r \begin{pmatrix} 1 - \tilde{v}_{11}\chi_1 & -\tilde{v}_{12}\chi_2 \\ -\tilde{v}_{21}\chi_1 & 1 - \tilde{v}_{22}\chi_2 \end{pmatrix}. \tag{8}$$

The individual layer susceptibilities can be determined from the well known expressions given by Stern [42]. From (7), we can determine the screened component v_{12} and hence determine the matrix element $M_{1,2,1',2'}$. It is also clear that the result cannot depend on whether the interaction is attractive (electron-hole) or repulsive (electron-electron and hole-hole). We thus see that within Random Phase Approximation (RPA), the (minor) differences between the EHBL and a 2x2DEG can arise from the difference in their band effective masses and the shape of the subband wavefunction for the holes. As far as the authors understand, the only way to appreciate (theoretically) the crucial difference between attractive and repulsive interaction within Born approximation is to take the next step to RPA by introducing the "local-field corrections".

RPA is known to fail for $r_s > 1$. By the inclusion of a local-field correction $G_{ij}(q)$, the short-range potentials can be improved upon $(v_{ij}(q)(1 - G_{ij}(q)))$. One approach to solving for $G_{ij}(q)$ is the Hubbard approximation [12] that includes the effect of exchange. The potentials can also be calculated self-consistently using Singwi et al. (1968) [13] (STLS) approach. This was done for the electron-electron and electron-hole bilayer by Świerkowski et al. [16, 43], who found that STLS gave a significant drag enhancement over the RPA, due to the effect of short-range correlations.

The drag resistivity in an EHBL was predicted to be larger than the electron-electron bilayer for three reasons, with the

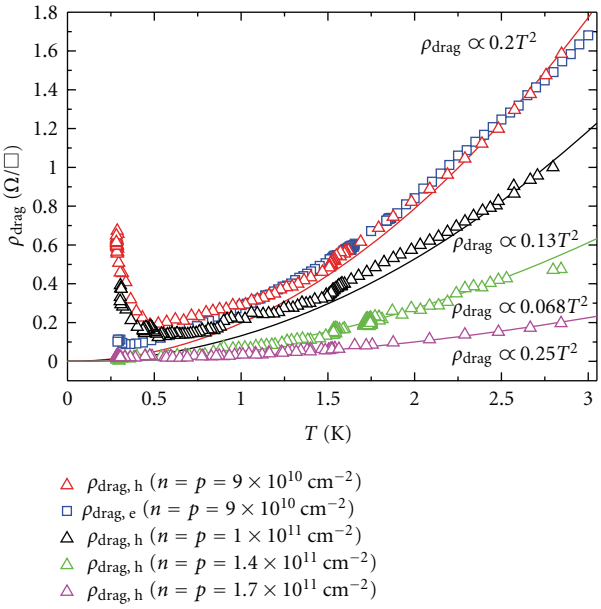

FIGURE 9: Hole drag resistivity versus temperature shown for $n = p = 9, 10, 14, 17 \times 10^{10}$ cm^{-2}, down to 300 mK. Electron drag is only shown for $n = p = 9 \times 10^{10}$ cm^{-2} for clarity. (Device: B138/C4-1-10 nm Barrier). The drag voltage was measured in two ways, by sending current through the electrons and measuring the open-circuit voltage across the holes ($\rho_{drag,h} = V_h/I_e$) or by sending current through the holes and measuring the voltage across the electrons ($\rho_{drag,e} = V_e/I_h$). As long as the current is low enough so that the system is in the linear response regime, thermodynamic arguments [54] predict that $\rho_{drag,e} = \rho_{drag,h}$.

larger hole mass responsible for two. First, the excitations in the EHBL are lower in energy, as T_F is lower for the heavier hole layer. Second, the intralayer correlations are larger in the heavier hole layer (greater r_s), which reduces the interlayer screening. The third contribution arises from the attractive interlayer interaction in the EHBL that enhances the interlayer correlations (larger pair-correlation function $g(r)$ for small r), with the opposite effect in the repulsive electron-electron bilayer. Subsequently, the interlayer local-field correction in the EHBL is negative whereas in the electron-electron case, it is positive. Hence, the modified potential in the EHBL is *larger* leading to an increased drag resistivity.

If the determinant of $\epsilon(q, \omega)$ vanishes then those regions can make large contributions to ρ_{drag}. These are the plasmon modes of the bilayer. The location of the (two) plasmon branches with respect to the single-particle excitation spectrum of the particles in the two layers in the (q, ω) plane, is an important aspect of the physics of the bilayer. These modes were studied (within RPA) by Das Sarma and Madhukar (1981) [44] and Hu and Wilkins (1991)[45]. Later work of Liu et al. (1996) [17] and Hwang and Das Sarma [41] that go beyond RPA has also highlighted how the plasmon contribution can differ in 2x2DEGs and EHBLs. However, it is not possible to get a finite drag at $T = 0$ due to contributions from the plasmon modes.

Yurtsever et al. (2003) [38] compared the 2x2DEG drag data of Kellogg et al. [46], with RPA, STLS, and their own method based on the Hubbard approach. The RPA and TF underestimate the drag whereas the STLS method gives an overestimate of the drag. Good agreement with their Hubbard model was found. Similar work was done by Hwang et al. (2003) [47] looking at data from 2x2DHG of Pillarisetty et al. [48] that had a drag resistivity 2-3 times larger than drag in corresponding electron-electron bilayers [46]. They used the Hubbard approximation and included scattering with $q \sim 2k_F$, appropriate for large r_s, and phonon-mediated drag. A deviation from T^2 was found ($T^{2.4}$) as $T \approx T_F$ for the holes and an enhanced phonon contribution for the hole-hole bilayer compared to the electron-electron system. The intralayer correlations are dependent on r_s which affects the screening at low densities. A comprehensive comparison of the predictions of various local-field theories, and the Fermi hypernetted chain approximation for Coulomb drag has been done by Asgari et al. [39], more recently.

For the RPA, STLS, and Hubbard methods, a stronger dependence on density is predicted, $(n_1 n_2)^{-2}$ [38] (rather than $(n_1 n_2)^{-3/2}$ for the TF model [5]), which has been observed [46]. The T^2 relationship is only exact in 3D. For 2D, there exist corrections from the divergences in phase space for $q \sim 0$ and $2k_F$, corresponding to forward and backward transitions on the Fermi surface. A correction proportional to $T^2 \ln T$ is expected [49], but should be small. This correction is believed to have been observed in low-density electron-electron bilayers [46].

A similar temperature dependence of $-T^2 \ln(T/T_\tau)$ ($T_\tau \equiv \hbar/k_B\tau$) is expected [50], when a large amount of disorder ($l < d$, where l is the mean free path) is included at very low temperatures.

Hwang and Das Sarma [41], calculated the drag resistivity (and single-layer resistances) for EHBLs with parameters fitted to the devices of Seamons et al. [51, 52], with 20 nm and 30 nm barriers. Using local-field corrections and dynamical screening, they were able to show that the coupled bilayer plasmon modes in the EHBL greatly enhance the drag resistivity with respect to the electron-electron and hole-hole bilayers.

5. Coulomb Drag in Electron-Hole Bilayer: Experimental Results

Coulomb drag at $T < 1$ K in EHBLs in a regime where $d/l \sim 1$, has recently been measured by the authors' group and an experimental group in Sandia [51, 53]. Our results show that drag measured in a device with a 10 nm $Al_{0.9}Ga_{0.1}As$ barrier (device B138/C4-1) is shown in figure 9 for matched electron and hole densities ($n = p$). For the two highest densities ($n = p = 1.4, 1.7 \times 10^{11}$ cm^{-2}), the hole drag resistivity is monotonic over this temperature range and appears to go towards zero as the temperature does. However, for the lower-density traces ($n = p = 9, 10 \times 10^{10}$ cm^{-2}), an upturn is seen in the hole drag. The lower-density trace has a larger upturn and the corresponding electron drag trace ($n = p = 9 \times 10^{10}$ cm^{-2}) is also shown. Only a very

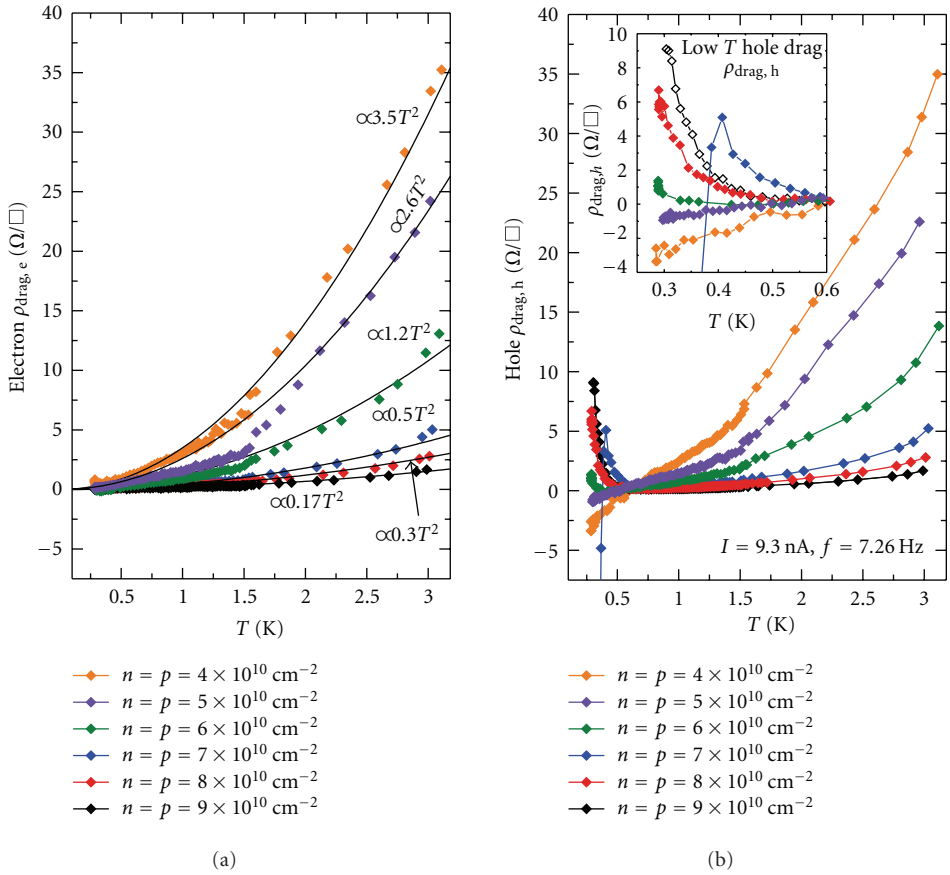

FIGURE 10: Drag resistivity measured on electron (a) and hole layer (b) versus temperature for $n = p = 4, 5, 6, 7, 8, 9 \times 10^{10}$ cm^{-2}, down to 300 mK. (Inset) Expanded low-temperature drag resistivity measured on hole layer. For the lowest density, $k_F d \approx 1.25$, $r_{s,e} = 2.8$, and $r_{s,h} \approx 14.1$. (Device: B138/C4-2-10 nm Barrier).

small upturn (if any) is found in the electron drag, with $\rho_{\text{drag},h} \neq \rho_{\text{drag},e}$ below ~1 K.

In another 10 nm barrier device (B138/C4-2) fabricated from the same wafer (I.D. A4268), lower-matched densities could be reached. Electron and hole drag resistivities are shown in Figure 10 for $n = p$ between 4 and 9×10^{10} cm^{-2}. The high-temperature drag is a good fit to T^2 and $\rho_{\text{drag},h} = \rho_{\text{drag},e}$. For 9×10^{10} cm^{-2}, the T^2 coefficient is similar ($\sim 0.2\,\Omega/\square\text{K}^{-2}$) to the first device B138/C4-1 (see Figure 9). At lower densities (Figure 10), the upturn does not increase (as seen in Figure 9) but becomes smaller, with the lowest two densities ($4, 5 \times 10^{10}$ cm^{-2}) displaying no upturn at all and a *sign-reversal* at the lowest temperatures. For an intermediate density 7×10^{10} cm^{-2}, the upturn is followed by a sharp negative downturn around 300 mK. In contrast, the electron drag resistivity remains monotonic and follows the expected T^2 dependence for two Fermi liquids. It is interesting to note that the departure from the T^2 dependence in the hole drag is relatively insensitive to density and occurs at ~700 mK. Note that at $n = p = 4 \times 10^{10}$ cm^{-2}, $d/l \approx 0.5$ is reached.

Nonreciprocity at low temperatures is an unexpected and puzzling result, since the drag is clearly in the linear regime. The drag resistivity was found to be independent of the excitation current frequency, up to ~100 Hz. Switching the grounding point between the layers can detect whether the measurement circuit is equivalent in the two drag configurations. Shifting the grounding and bias points was found not to affect the anomalous low-temperature data. At higher temperatures, the drag is reciprocal, this too verifies that the measurement circuit is set up correctly. The following section reports drag measured in EHBL devices below 300 mK in a dilution refrigerator.

5.1. Coulomb Drag down to 50 mK. Coulomb drag in sample B138/C4-1 was measured down to 50 mK. In Figure 11, drag is shown for $n = p = 9, 11 \times 10^{10}$ cm^{-2}. For the 9×10^{10} cm^{-2} traces, the high-temperature dependence is similar to that in Figure 9 measured in a different system. An upturn in the hole drag is seen, which appears to be larger for the lower density. Deviation from T^2 appears at a higher temperature for the lower density. However, for this density, below 250 mK the hole drag peaks and starts falling. A smaller upturn is seen in the electron layer, despite the I-V plot (Figure 11(b)), showing that the electron drag is still linear down to lower excitation currents (0.5 nA).

In a 25 nm barrier, undoped device (B135/C3-4) with resulting higher hole mobilities, the drag resistivity measured down to 35 mK is shown in Figure 12 for

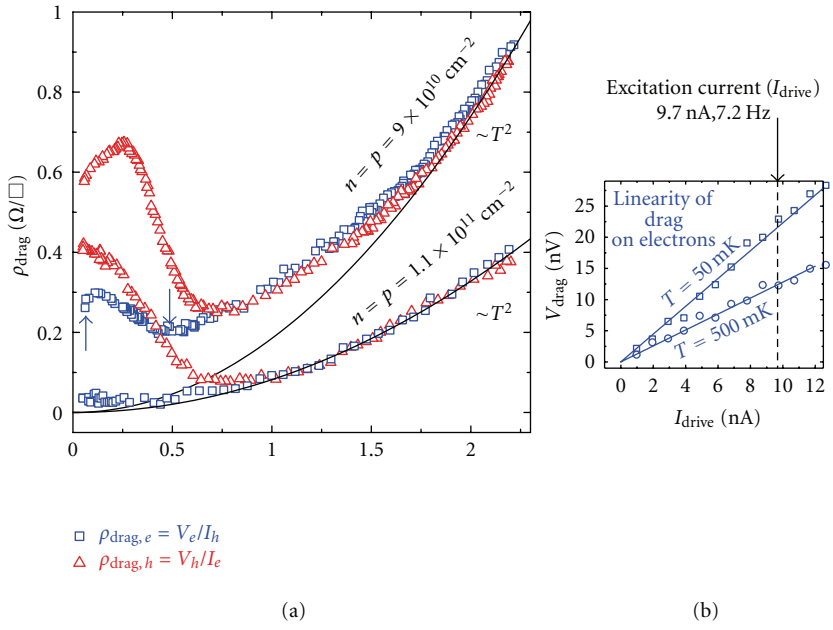

FIGURE 11: (a) Electron and hole drag resistivities versus temperature for $n = p = 9$ and 11×10^{10} cm^{-2} versus temperature, down to 50 mK. T^2 coefficients are 0.08 and 0.19 Ω/□K^{-2}, respectively. (b) I-V trace for drag on electron layer for $n = p = 9 \times 10^{10}$ cm^{-2}, indicated by arrows (a). Electron and hole layer mobilities at $T = 1.5$ K, $\mu_e = 1.5 \times 10^6$ cm^{2}V^{-1}s^{-1} and $\mu_h = 1.1 \times 10^5$ cm^{2}V^{-1}s^{-1}. (Device: B138/C4-1-10 nm Barrier).

$n = p = 7, 11 \times 10^{10}$ cm^{-2}. For the lower-density traces, an upturn is seen in the hole drag, though it peaks, then falls and below 200 mK saturates at a small negative value. As shown in Figure 12(b), even the negative hole drag appears to be linear down to small currents. But the corresponding electron drag trace still appears to follow the T^2 dependence. The features in the low-temperature drag are not hysteretic with temperature. All points were taken as the sample was cooled, except the I-V traces that were taken as the sample was warmed. The resistances corresponding to these traces are shown as black circles in Figure 12 and agree well with the other data. Figure 12(c) shows the in- and out-of-phase component of the hole drag signal for $n = p = 7 \times 10^{10}$ cm^{-2}. This shows no anomalies in the out-of-phase signal coincident with the anomalous behaviour seen in the in-phase signal, ruling out artefacts from capacitive effects or ohmic contact failure. For the higher-density traces ($n = p = 1.1 \times 10^{11}$ cm^{-2}), a small upturn in the electron drag is seen whereas a small negative downturn is seen in the hole drag (see inset, Figure 12).

For an excitonic superfluid phase, an upturn in the drag is predicted that would diverge, approaching the single-layer resistivities [6], which themselves would diverge as the number of unpaired electrons and holes that are able to carry single-layer current fall. But such a strong effect is not seen. Besides in the excitonic phase, there is no reason to expect Nonreciprocity. Electrostatic binding within an exciton may explain the upturn seen in the drag and departure from the behaviour expected for weak particle-particle scattering. However, an excitonic phase is unlikely to have a preference for the lighter or heavier layer and cannot account for the lack of reciprocity seen at low temperatures. An indicator for the presence of excitons would be an enhancement of the drag at $n = p$, particularly for a BCS-like state where nesting of the electron and hole Fermi surfaces is required.

5.1.1. High-Temperature T^2 Dependence. The magnitude of drag in the EHBL is expected to be greater than in electron-electron and hole-hole bilayers, due to the additional plasmon enhancement [41] and due to larger correlations between the layers [55], including the high-temperature ($\sim T^2$) regime. The T^2 coefficient ($\rho_{drag} = AT^2$) for the data in Figure 10 (10 nm barrier) can be compared with that for 10 nm barrier electron-electron and hole-hole bilayers. The electron-electron data of Kellogg [56] for $n_1 = n_2 = 5 \times 10^{10}$ cm^{-2} gives a coefficient of $A = 0.3\,\Omega/\square K^{-2}$, compared to $A \approx 2.6\,\Omega/\square K^{-2}$ in the EHBL. This shows an enhancement by a factor of ~9. In the hole-hole bilayer of Pillarisetty et al. [48], for $p_1 = p_2 = 7 \times 10^{10}$ cm^{-2}, $A \approx 0.7\,\Omega/\square K^{-2}$ compared to $A \approx 0.5\,\Omega/\square K^{-2}$ in the EHBL. These are similar, despite the hole-hole bilayer having a larger r_s in both layers. However, at these densities, for an accurate comparison, the correction to account for the different r_s must be made.

Comparing the data in Figures 10 and 12 for 10 nm and 25 nm barrier devices at $n = p = 7 \times 10^{10}$ cm^{-2}, the dependence on interlayer separation d can be examined. The respective T^2 coefficients are $A = 0.5\,\Omega/\square K^{-2}$ and $A = 0.051\,\Omega/\square K^{-2}$, a ratio of ~10. By measuring the interlayer capacitance, the wavefunction peak to peak d can be estimated. The 10 nm and 25 nm barriers correspond to d of 25 nm and 40 nm, respectively. From (3), one expects $A \propto d^{-4}$. Hence, an expected ratio of

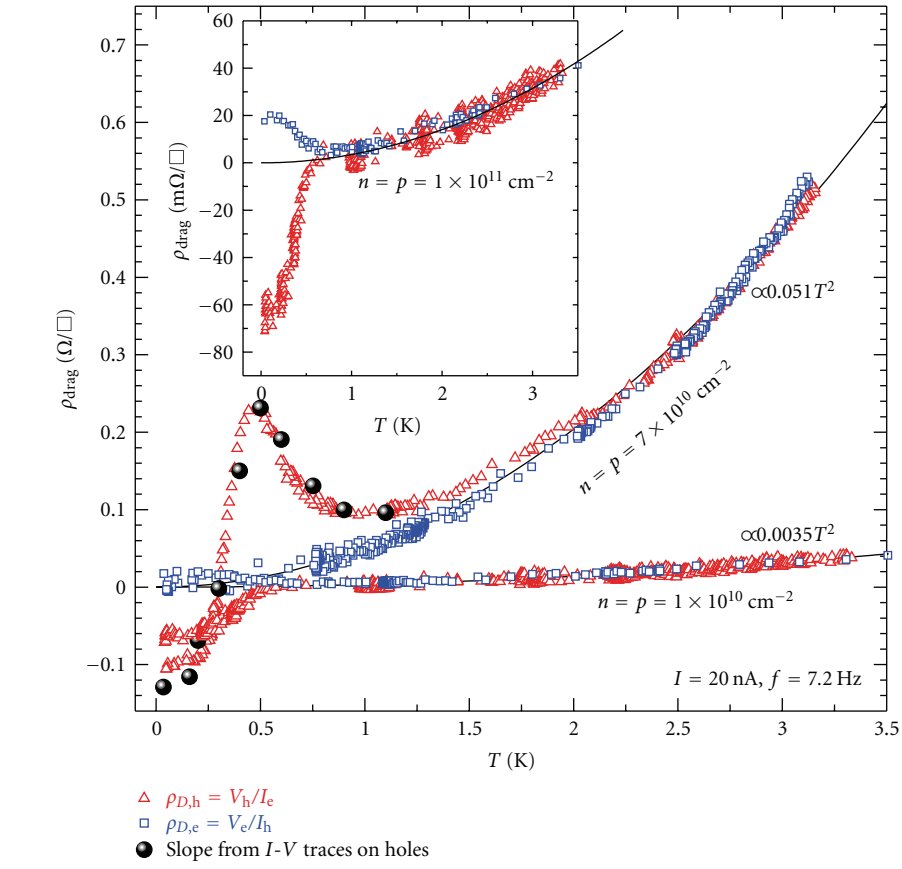

(a)

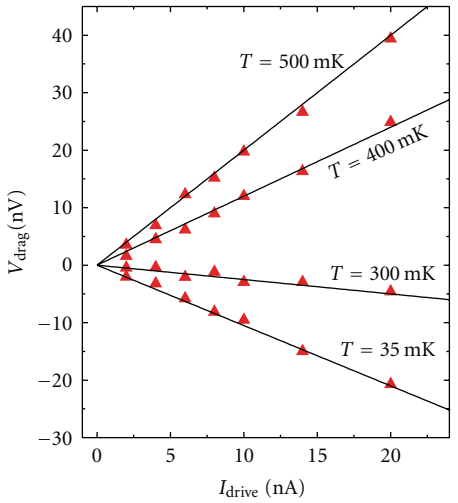

(b)

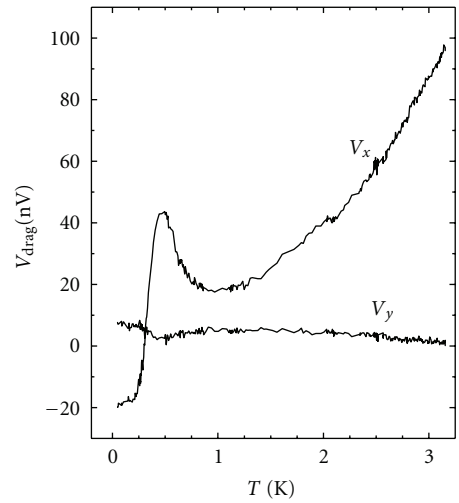

(c)

FIGURE 12: (a) Electron and hole drag resistivity versus temperature for $n = p = 7$ and 11×10^{10} cm^{-2} versus temperature, down to 50 mK. T^2 coefficients are 0.0035 and 0.051 Ω/□K^{-2}, respectively. (b) I-V (a.c. $f = 7.2$ Hz) trace for drag on hole layer for $n = p = 9 \times 10^{10}$ cm^{-2} at temperatures indicated. The resistances found from these slopes are displayed on (a). (c) In- and out-of-phase components of the drag voltage (V_{drag}) for the $n = p = 7 \times 10^{10}$ cm^{-2} trace. Electron and hole layer mobilities for $n = p = 7 \times 10^{10}$ cm^{-2} at $T = 1.5$ K; $\mu_e = 6.8 \times 10^5$ cm^{2}V^{-1}s^{-1} and $\mu_h = 3.3 \times 10^5$ cm^{2}V^{-1}s^{-1}. (Device: B135/C3-4-25 nm Barrier).

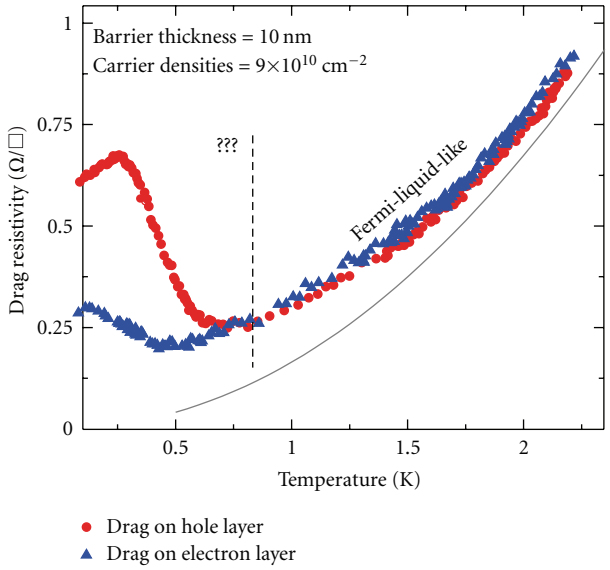

Figure 13: Electron (blue) and hole (red) drag resistivity versus temperature for $n = p = 9 \times 10^{10}\,\mathrm{cm}^{-2}$, down to 50 mK. The data of Figure 11 is reproduced along with the result of the calculation (solid line) described in the text. We considered a cosine wavefunction for the holes and a Fang-Howard type wavefunction for the electrons.

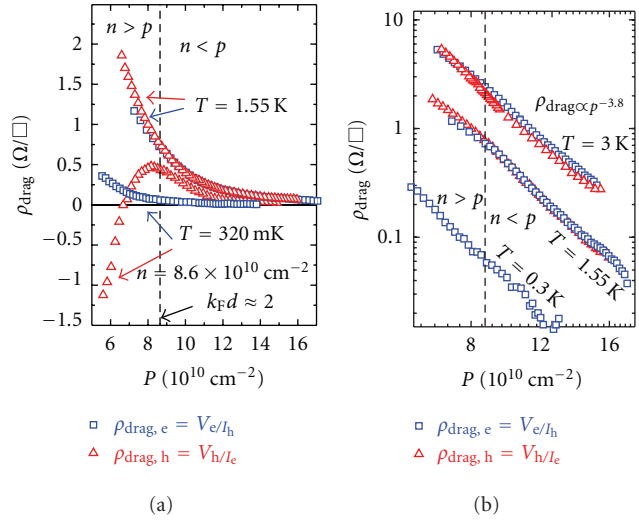

Figure 14: Electron and hole drag resistivities with electron density held constant at $n = 8.6 \times 10^{10}\,\mathrm{cm}^{-2}$ versus hole density at $T = 320$ mK, 1.55 K, and 3 K. (Device: B138/C4-1-10 nm Barrier).

$d^4_{(25\,\mathrm{nm})}/d^4_{(10\,\mathrm{nm})} = 40^4/25^4 = 6.6$, close to the measured 10. An increase in interlayer correlations with reducing separation may explain the enhancement over the expected value. The density dependence of the T^2 coefficient is examined next.

We have been able to describe our high-temperature (above 1 K) drag measurements using the linear Boltzmann formalism as in (2), provided that the average intralayer particle spacing is smaller than the average interlayer particle spacing. We used a simple model with temperature-dependent Lindhard functions and accounted for the finite-thickness of the wavefunctions. Intralayer correlations were taken into account using a Hubbard local-field correction as described by Yurtsever et al. [38], but interlayer correlations were neglected. We also neglected phonon effects. This model works well for 10 nm and 25 nm barrier devices at high enough densities (see Figure 13). For very low densities, the model underestimates the drag, suggesting that interlayer local-field corrections might be large because particles in different layers are closer together than particles in the same layer. We have also noticed that the calculated drag is sensitive to the shape of the wavefunction. However, the low-temperature drag observations cannot be explained by a Boltzmann-type even if local-field corrections are taken into account.

5.2. Drag at Mismatched Densities. Data at constant electron density ($n = 8.6 \times 10^{10}\,\mathrm{cm}^{-2}$) with p varied, is shown for device B138/C4-1 in Figure 14. At higher temperatures ($T = 1.55$ K and 3 K), where the anomalous drag is not seen, agreement is found between the electron and hole drags, and a good fit to a power-law dependence is found ($\rho_{\mathrm{drag}} \propto p^{-3.8}$). At the lowest temperature, the electron drag still has the same power-law dependence on p. However, as p is lowered the hole drag no longer agrees with the electron drag, and exhibits the upturn found in Figure 9 at $n = p = 9 \times 10^{10}\,\mathrm{cm}^{-2}$. A maximum is seen in the hole drag close to $n = p$, but for $n > p$ a sharp downturn that goes *negative* is found. It is unclear from these observations whether $n = p$ or the value of the hole density ($k_F d \approx 2$, transition to large-angle scattering) is important, and more work is required to analyse this point. However, achieving the upturn is not dependent on matching the densities exactly. This point was also investigated by Morath et al. [52]. While a peak is seen in the hole drag close to matched densities (Figure 14), it cannot be concluded that this is excitonic (or phonon/plasmon) in origin.

Considering the data in Figure 10 for $n = p$, the T^2 coefficients are plotted against layer density ($\rho_{\mathrm{drag}} = AT^2$) in Figure 15. A power-law dependence for $A \propto n^a p^b$, with $a + b = -4.0$ is found. This total has been predicted by the RPA, Hubbard-like and STLS calculations performed by Yurtsever et al. [38] for the electron-electron bilayer. These go beyond the (high-density) weak coupling limit (TF) where $(np)^{-3/2}$ is predicted (3). In Figure 14, a dependence of $\rho_{\mathrm{drag}} \propto p^{-3.8}$ is found, which together implies a weaker dependence ($|a| < |b|$) on n rather than p. For drag taken when the hole density is held constant at $p = 1.5 \times 10^{11}\,\mathrm{cm}^{-2}$ and the electron density is varied (data not shown), the T^2 coefficient is plotted in Figure 15 against n, showing $A \propto n^{-0.5}$. Some inaccuracy will occur as the interlayer separation (d) is to some extent a function of the interlayer bias that determines the electron density. This effect was studied by Morath et al. [57]. Similarly, the position of the hole wavefunction will be affected by the backgate bias. Depleting holes will push the wavefunction peak towards the barrier. Nevertheless, it is expected that the drag will be more sensitive to the layer with greater r_s [47, 48]. Earlier work in the EHBL showed the

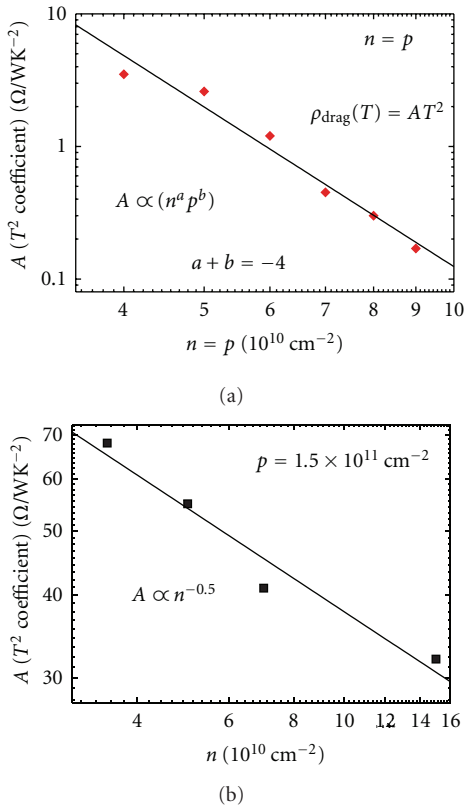

FIGURE 15: Fit for T^2 coefficient A for ρ_{drag} with p constant $p = 1.5 \times 10^{11}$ cm^{-2} and n varied (b) (data not shown). Same for $n = p$ (data shown Figure in 10) (a). (Device: B138/C4-1 (a), B138/C4-2 (b) −10 nm Barrier).

opposite result that the drag was found to be more sensitive to the electron density [19], but this work was performed above $T = 9$ K, where other processes such as phonon-mediated drag will be significant.

5.3. Interlayer Leakage. In all biased structures, finite leakage currents will exist. In the EHBL, the interlayer bias (∼1.5 V across ∼10 nm) acts across a small distance and measurable leakage exists, though it is typically far smaller than the measurement currents used. In the best devices, $I_{leak} \approx 100$ pA, while the measurement currents are typically between 0.5–10 nA. The effect of the leakage current on transport measurements is important, particularly if it can influence the drag measurement or the state of the system. There are several possible mechanisms whereby leakage can influence measurements directly. Firstly, the electrons/holes that leak through the barrier will be much hotter than the 2DHG and 2DEG, which will have reached thermal equilibrium with the lattice. It must be possible for these energetic particles to lose this energy on a shorter timescale (thermalisation time) than the characteristic lifetime of any coherent phase existing in the bilayer, so that the leakage event will be forgotten quickly by the system. Likewise, the leakage events must be infrequent, relative to the phase lifetime (such as the lifetime of an exciton).

As discussed earlier, the leakage is most likely caused by barrier defects and carriers will probably lose energy via transitions through defect states that exist mid-gap. In this respect, backgate leakage is not likely to be as important. While much larger biases are used, a charged particle is unlikely to travel the distance from the backgate to the 2DHG ballistically, and energy will be dissipated to the lattice. It is necessary for the particles to be in local equilibrium for the true ground state to emerge, despite the two layers being at different electrochemical potentials. It is unknown how much leakage will affect this condition. For a superfluid-like state, the lifetime due to leakage between the layers must be larger than $\tau \sim \hbar/\Delta$, where Δ is the energy gap. For the effect of the gap to be observed, we need $T \lesssim \Delta/k_B$, which assuming a lowest measurable temperature of 50 mK, gives a bound of $\tau < 150$ ps. A typical interlayer leakage current in our device is ∼50 pA, over an area ($A_{overlap}$) of 0.14 mm^2 (including any leakage due to radiative recombination). The characteristic timescale between leakage events (how long the particle remains in one layer) is $\tau_{leak} = enA_{overlap}/I_{leak}$. Hence, an approximate leakage lifetime (for $n = p = 1 \times 10^{11}$ cm^{-2}) is $\tau_{leak} \sim 0.4$ s, which is much longer than any typical transport lifetime ($\tau_{drag} \sim 10$ ns, $\tau_{xx} \sim 10$ ps) in these devices and any lifetime corresponding to a gapped phase that could exist within the measured temperatures.

The drag resistivity at low temperatures is typically smaller than 1 Ω/□, and stray currents can adversely affect the measurement due to the larger single-layer resistivities. All measurements were conducted with a.c. phase sensitive detection. Incoherent d.c. leakage cannot contribute directly to an error in the measurement. However, a weak point in the barrier may allow a path for the a.c. excitation current to cross into the other layer and return via the interlayer bias supply (battery) (Figure 16), which appears to the a.c. as a low resistance path. As shown in Figure 16(a), by changing the interlayer biasing points, the effect can be reversed. For device B138/C4-2 at $n = p = 8 \times 10^{10}$ cm^{-2}, changing the bias has little effect on the Nonreciprocity or the upturn in the hole drag. The electron drag is also unaffected.

6. Discussion

Features are seen in the drag resistivity at low temperatures that cannot be explained within the framework of Fermi-liquid theory [41]. For two Fermi gases, the phase space allowed for interlayer particle-particle scattering must go to zero as the temperature does.

Qualitatively, similar anomalous behaviour is seen in two 10 nm barrier devices, with an upturn below 0.5 K that may be followed by a downturn or sign reversal at the lowest temperatures, for the lowest densities (Figures 10 and 14). The magnitude of the upturn differs by a factor of ten between devices (for the $n = p = 9 \times 10^{10}$ cm^{-2} at 300 mK, Figures 9 and 10), with the high-temperature drag ($\sim T^2$) agreeing well. This would suggest that sample-dependent factors such as disorder might be important in the anomalous regime. Anomalous behaviour also occurs at larger layer separations (25 nm barrier), consistent with the

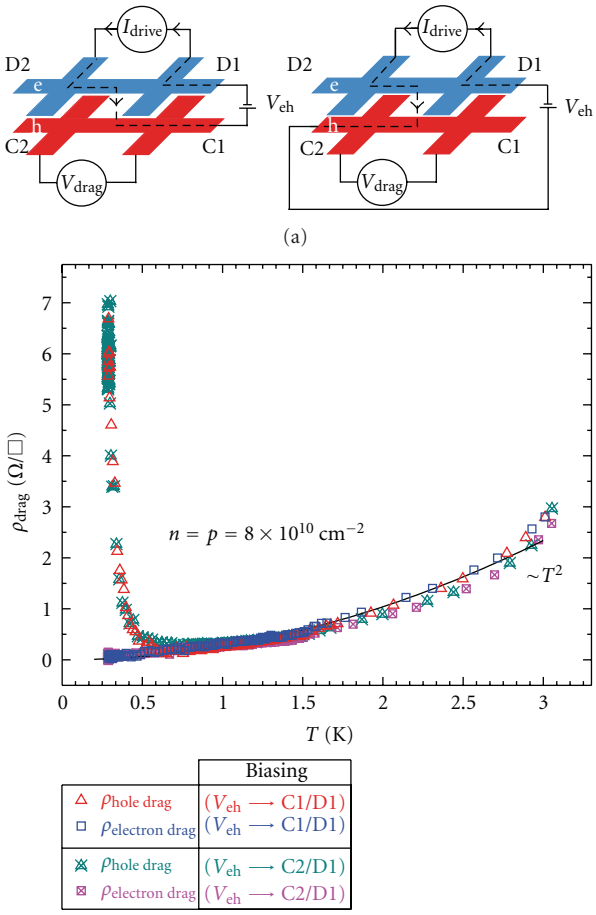

FIGURE 16: (a) Diagram showing that a sign reversal of the error in drag due to the excitation current leaking between layers is expected when biasing points (named C1, C2, D1, and D2) are altered, as the leakage current direction in the drag layer is changed. (b) Electron and hole drags for the two interlayer biasing configurations, for $n = p = 8 \times 10^{10}$ cm^{-2}. (Device: B138/C4-2-10 nm Barrier).

findings of Seamons et al. (2009) [51], where a small upturn was found in 20 nm barrier samples but not for 30 nm.

Third-order corrections to the interlayer interaction by Levchenko and Kamenev [58], showed that nonzero drag at $T = 0$ was possible, and so does not necessarily indicate the presence of strong interlayer correlations. However, the effect they find is small ($\sim 10^{-4}\,\Omega$/W), particularly for high-mobility samples, and cannot explain the anomalous drag seen ($\sim 1\,\Omega$/W).

The deviation is too large to be caused by a plasmon or phonon enhancement [28, 36], which would be peaked at matched densities and higher temperatures. Plasmon enhancement is expected at $T \sim 0.2T_F$ ($T_{F,e} > 16$ K, $T_{F,h} \gtrsim 3$ K), while below the Bloch-Grüneisen temperature (~ 1 K), the phonon contribution is heavily suppressed.

6.1. Coulomb Drag Upturn. The upturn in the Coulomb drag (Figure 9) at the lowest temperature, may be a signature of an increased interlayer coupling due to the formation of excitons. This coupling is not suppressed by the falling phase space with temperature, restricting scattering at the Fermi surfaces. Within the exciton regime, distinct Fermi surfaces no longer exist when the binding energy exceeds k_BT, lifting this phase-space restriction.

The transition temperature for an excitonic superfluid state (assuming a 2D Kosterlitz-Thouless type transition), is expected to increase with exciton density (in 2D $T_c = n_{ex}\hbar^2/0.71m^*_{ex}k_B$, (1)), where n_{ex} is the exciton density. Seamons et al. [51] attempted to identify the temperature of the minimum in the drag as the transition temperature, arguing that this point occurs at higher temperatures for larger densities. It is possible to see the same trend in Figures 9 and 11, though in the latter the deviation from T^2 clearly occurs at a higher temperature for the lower-density data ($n = p = 9 \times 10^{10}$ cm^{-2}). This point of deviation may be more significant than the drag minimum.

However, the upturn is far smaller than that predicted for an excitonic state [6, 8, 10]. The drag is anticipated to reach a value approaching the single-layer resistivities, with a sharp change (discontinuity) signifying the phase transition (unless only a small fraction of electrons and holes enter a paired state). Hu [8] predicted an enhancement due to electron-hole pair fluctuations above the transition rising as $\sim T^2/\log(T/T_c)$. Fitting this to an upturn to obtain T_c is possible (Morath et al. (2009) [52]), but it cannot explain the subsequent downturn seen in Figures 11 and 12. The prefactor to the expression predicted by Hu [8], is larger (by a factor of $\sim$1000) than the upturn measured [52]. For the drag at mismatched densities (Figure 14), the peak expected at $n = p$ is not seen. The peak in the figure is not sharp enough and is asymmetric. As discussed earlier, it is unclear whether $n = p$ or k_Fd plays a role in the peak. Crucially, matched densities are not necessary to see the upturn.

Other indicators for an excitonic phase could include a temperature dependent Hall voltage, since neutral excitons would not feel the Lorentz force. The authors had looked for this effect, but not observed it in their experiments.

6.2. Coulomb Drag Sign Reversal. At the lowest temperatures, in 10 nm and 25 nm barrier samples, a sign reversal of the drag resistivity has been seen. In this situation, driving the current in one layer in one direction causes particles in the other layer to move in the *opposite* direction. Sign reversal has been seen for drag between layers at large filling factors (moderate magnetic fields) in the quantum Hall regime [59–63]. Partly filled Landau levels, possess electron and hole character. If the highest Landau levels in the drag and drive layers have opposite deviation from half filling, then ρ_{drag} is negative (electron-hole like) at low temperatures. At higher temperatures when k_BT is larger than the disorder broadened width of the Landau level ($\hbar/\tau$), then the drag returns to the zero magnetic field (positive) sign. For nonzero drag, the excitations at the Fermi surface must not have particle-hole symmetry [60, 63]. At the centre of a disorder broadened Landau level, this symmetry is acquired and the drag goes to zero. Varying the magnetic field will change the Landau level

populations and a complex series of positive and negative drag oscillations results.

Figure 12 shares many of the features seen in the temperature dependence of magnetodrag in an electron-electron bilayer [63] at $\nu = 7.7, 9.5$, where a peak is followed by a downturn. It is not immediately clear how the banding (density of states) required for this would occur at zero magnetic field. For 2DHG and 2DEG, $E(k)$ is expected to be continuous and the concept of disorder broadening cannot be applied.

Alkauskas et al. (2002) [64] have proposed that a sign reversal in the drag resistivity may result from the inclusion of an in-plane periodic potential, with wavelength much greater than that of the underlying atomic lattice. This extra periodicity creates an additional Bragg plane and the formation of minibands, with a bandgap at much smaller k, at the Brillouin zone boundary corresponding to the large wavelength of this additional potential. They found that as the density was increased, a sign reversal would occur. Normally, particles exist within the parabolic bottom of the band and are scattered before they reach the zone boundary. If the Brillouin zone is smaller, then the point at which $\partial^2 E/\partial k^2$ $(= \hbar^2/m^*)$ changes sign is attainable at experimental densities, leading to a sign change in the effective mass and a sign reversal in the drag resistivity. But for this to be relevant, a periodic solid-like phase must appear in the EHBL. Candidates for this include the Wigner crystal, where one or both layers has crystallised into a periodic array overlaying each other [65] or a spontaneous periodic modulation in charge density, known as a charge density wave [55]. These possibilities would be discussed further in the context of the single-layer resistivity measurements.

6.3. Drag Reciprocity. It is expected that for measurements in the linear regime, the hole and electron drag resistivities should be equal [54, 66, 67]. At the lowest temperatures, where the deviation from T^2 is found, a Nonreciprocity between $\rho_{\mathrm{drag},e}$ and $\rho_{\mathrm{drag},h}$ is observed, despite the measurements appearing to be in the linear regime. The measurement circuit is not the cause of the Nonreciprocity as the drag is reciprocal at higher temperatures. The effect of interlayer leakage was discussed before as a possible source of error, but in our experiments, we have verified that this gives no noticeable contribution (Figure 16).

Measurements of Coulomb drag down to 300 mK on EHBLs has been performed by Seamons et al. (2009) [51, 52], on samples with 20 nm and 30 nm barriers and similar densities. For the narrower barrier, a small upturn is found only in the drag measured on the holes ($\sim 0.4\,\Omega$/W). This Nonreciprocity was explained as a result of additional Joule heating caused by passing current through the more resistive hole layer for the electron drag configuration. They report saturation in the electron Shubnikov-de Haas oscillations at about 1 K, when the same current used for drag is passed through the hole layer. Single-layer measurements reported by Seamons et al. on the hole layer require a much smaller current than that used for drag, so heating was avoided.

Joule heating cannot explain the Nonreciprocity found in this work. Heating will be a nonlinear effect ($\sim I^2$R), but no nonlinearity is found in the I-V traces of the drag resistivity. For the data taken in Figure 9 at $n = p = 9\times10^{10}$ cm^{-2}, at the lowest temperature, the two-probe resistance of the electron and hole layers differed by a factor of 9 (hole 2-probe 62 kΩ, electron 2-probe 7.2 kΩ). The two and four-probe (single-layer) resistances of the hole and electron layers are shown in Figure 17 as a function of temperature. Reducing the current by a factor of three will give the same Joule heating for the electron drag configuration as for the hole drag. But nonlinearities are not seen in this range (Figure 9). Indeed the same currents were used for single-layer measurements as for drag and no saturation of Shubnikov-de Haas amplitude with temperature was seen.

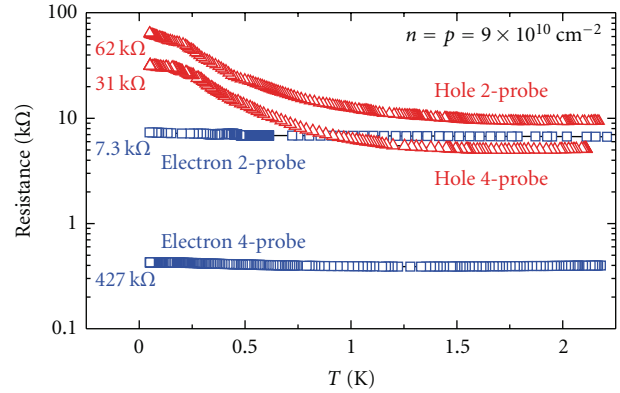

Figure 17: Two-probe and four-probe resistance of the electron (blue squares) and hole (red triangles) layers versus temperature, at $n = p = 9 \times 10^{10}$ cm^{-2}. (Device: B138/C4-1-10 nm Barrier).

7. Features in Single-Layer Resistivity: An Interaction-Driven Insulating State

In our EHBL devices it is possible to perform experiments with only the 2DHG present. This is achieved by keeping the interlayer bias below the threshold for electron accumulation ($V_{\mathrm{eh}} \approx 1.55$ V) and biasing both backgates negatively to induce holes in the QW. The hole density can then be controlled with the central backgate V_{bg}. The temperature dependence (0.3 to 1.5 K) of the single-layer resistivity of the holes is shown in Figure 18(a). As the density is lowered, there is a transition from metallic to insulating behaviour between 5 and 6×10^{10} cm^{-2}. These features are consistent with results from several 2DMIT studies of Silicon MOSFETs and GaAs/AlGaAs-based devices. The crossover occurs as expected close to $\rho_{xx} \approx h/e^2$ or equivalently to $k_F\ell = 1$, with $d\rho_{xx}/dT > 0$ for $\rho_{xx} < 25.8\,\mathrm{k\Omega}/\square$ and $d\rho_{xx}/dT < 0$ for $\rho_{xx} > 25.8\,\mathrm{k\Omega}/\square$. At $k_F\ell = 1$, the mean free path (ℓ) is approximately equal to the interparticle separation (l). Non-monotonic behaviour is observed for the $p = 6 \times 10^{10}$ cm^{-2} trace, which is insulating above $T \sim 0.8$ K and metallic below. This has been observed before in 2DHGs [68] and in an EHBL with a 30 nm barrier [57] and can be explained within Fermi liquid theory [69].

Most striking is the change in behaviour of the hole layer with the addition of the electron layer (kept in an

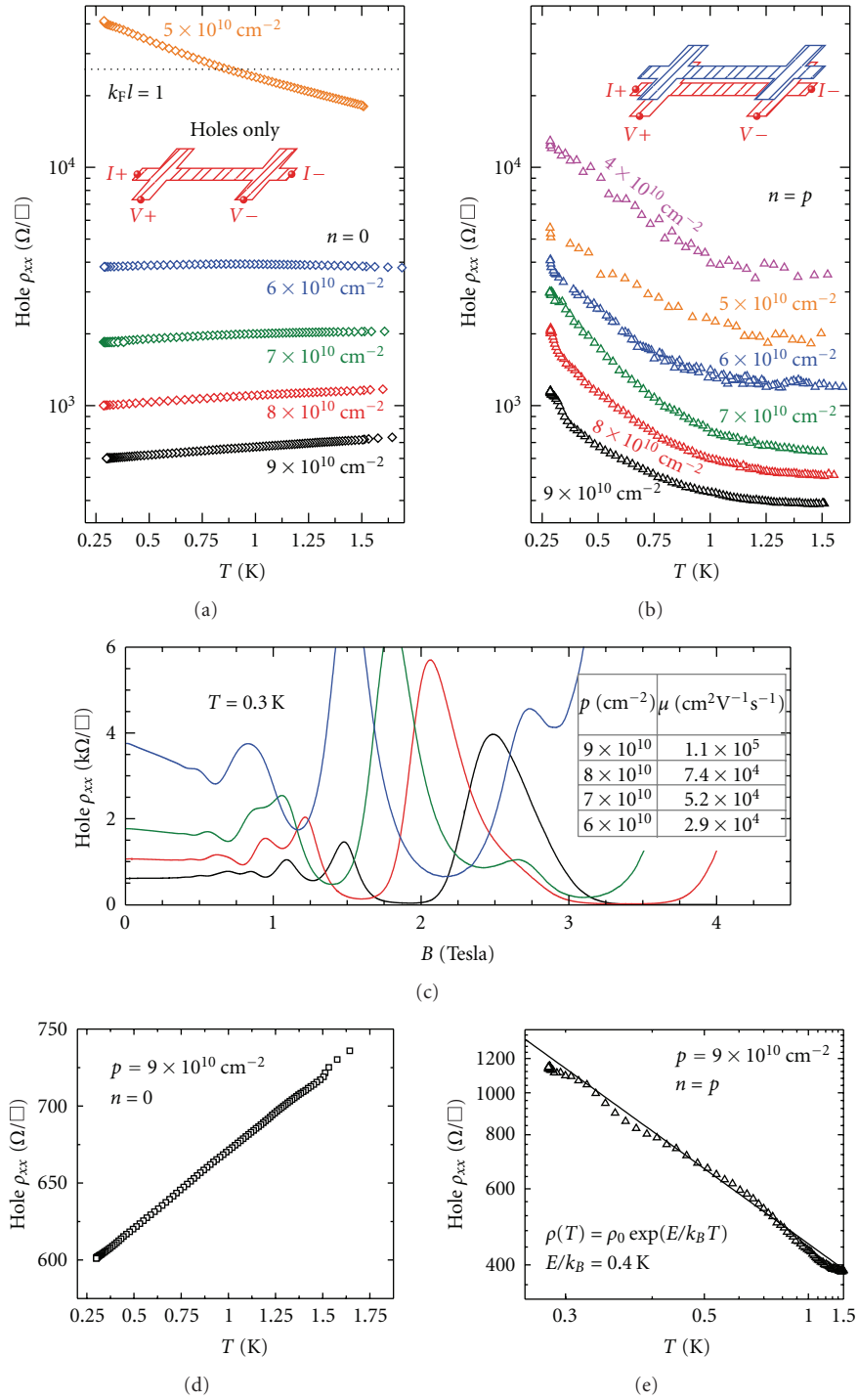

FIGURE 18: Resistivity of hole layer versus temperature for $p = 5, 6, 7, 8, 9 \times 10^{10}$ cm^{-2} at $B = 0$, (a) without electrons ($n = 0$) and (b) with electrons ($n = p$). (c) Magnetoresistance $\rho_{xx}(B)$ of hole layer for $p = 6, 7, 8, 9 \times 10^{10}$ cm^{-2} with no electrons present ($n = 0$), at $T = 0.3$ K. (d) "Metallic" hole layer $\rho_{xx}(T)$ for $p = 9 \times 10^{10}$ cm^{-2}, $n = 0$. (e) Arrhenius plot ($\ln(\rho)$ against $1/T$) for "insulating" hole layer $\rho_{xx}(T)$ with $n = p = 9 \times 10^{10}$ cm^{-2}, showing good fit to an exponential rise. (Device: B138/C4-2-10 nm Barrier).

open-circuit configuration), [70, 71] shown in Figure 18(b). All traces are now clearly insulating by $T \sim 1$ K, *even* those that had been metallic. This insulating state is occurring at $k_F \ell > 50$, with resistivity at $T = 1.5$ K far below the regime where a transition to insulating behaviour is expected. Localisation due to background disorder (impurities/dopants/defects) cannot account for this because the 2DHG sees the same disorder with and without the 2DEG present. Placing a plane of mobile charge next to the 2DHG is expected to improve the hole mobility. Adding

the electrons does result in a significant three-fold increase in hole mobility at $T = 1.5$ K; for $p = 6\times10^{10}$ cm^{-2}, $\rho_{xx,\mathrm{hole}}(n = 0) = 3808\,\Omega/\square$ falls to $\rho_{xx,\mathrm{hole}}(n = p) = 1203\,\Omega/\square$. This is consistent with the results of Morath et al. [57], from a 30 nm barrier EHBL device, where the dependence of the hole mobility with electron density was explored. The effect is much larger here, possibly due to the smaller barrier.

Improvement of the high-temperature mobility is likely to be the result of several processes. Background impurities will be screened by the presence of the 2DEG. Inducing the electrons requires a large electric field across the barrier, and then to reach matched densities ($n = p$) a depleting backgate bias is also required. Both of these cause the wavefunction to be "squeezed" against the AlGaAs barrier, improving the screening as the holes become more greatly confined (though also potentially harming the mobility due to increased interface roughness scattering and the higher level of background impurities found in AlGaAs). In this regime, the hole mobility is limited by remote ionised impurity scattering caused by the intentional p-dopants (verified by comparison to undoped structures). The interlayer bias will pull the holes towards the barrier and increase the effective spacer thickness (between the 2DHG and dopants) and accordingly improve the mobility.

Placing a conducting electron layer close to the 2DHG will also improve the screening, as image charges will form in this layer. If the interlayer separation is d, then the dipolar field (charge and its image) will drop faster than $\sim 1/r$ at distances greater than $\sim d$. This effect has been studied in gated 2DEGs [72] and in double QW structures (2x2DHG) with $d \sim 50$ nm [73].

While the change at $T = 1.5$ K can be accounted for by a combination of effects, the insulating behaviour at low temperature is unexpected as these arguments always improve the intralayer screening and lower the effective r_s. Matthiessen's rule-based addition of scattering rates cannot explain the increase in mobility [74] at $T = 1.5$ K. Adding the contribution of the interlayer scattering rate to the impurity scattering rate will cause a reduction in mobility. Going from the situation of a single hole gas ($1/\mu_h^{sl}$) (where $\mu = e\tau/m^*$), whose mobility is primarily dictated by impurity scattering ($1/\mu_h^{\mathrm{imp}}$), to the mobility of the holes with the addition of the electron layer (bilayer configuration) ($1/\mu_h^{bl}$) must introduce a term corresponding to the presence of the electron layer ($1/\mu_h^{C}$) and so

$$\frac{1}{\mu_h^{sl}} = \frac{1}{\mu_h^{\mathrm{imp}}} \longrightarrow \frac{1}{\mu_h^{bl}} = \frac{1}{\mu_h^{\mathrm{imp}}} + \frac{1}{\mu_h^{C}}. \tag{9}$$

This must mean that $1/\mu_h^{\mathrm{imp}}$ is changing in the presence of the second layer. Note that $1/\mu_h^{C} = en\rho_{\mathrm{drag}}$ [74], where n is the density of the electron layer. The anomalous drag cannot account for the increase in $\rho_{xx}(T)$ at lower temperatures, as it is too small. This suggests that a new single-layer scattering mechanism has emerged due to the presence of the electron layer.

The insulating state is *also* seen in the electron layer. Figure 19 shows both electron and hole layer resistivities down to ~50 mK. Both layers exhibit a similar behaviour,

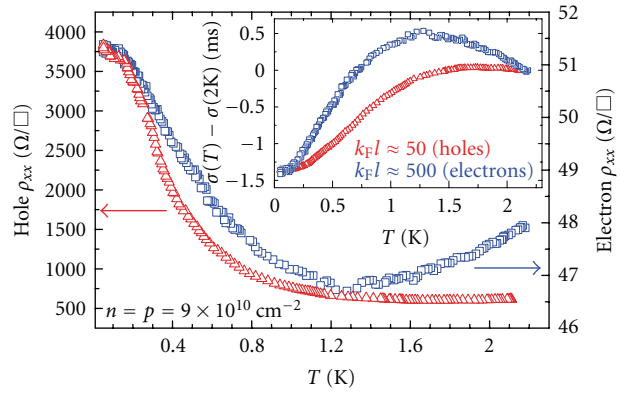

Figure 19: Resistivities of hole and electron layers versus temperature for $n = p = 9\times10^{10}$ cm^{-2}, down to $\approx$ 50 mK in a dilution refrigerator. At $T = 1.5$ K, $\mu_e = 1.5\times10^6$ cm^{2}V^{-1}s^{-1} and $\mu_h = 1.1\times10^5$ cm^{2}V^{-1}s^{-1}). (Inset) Change in conductivity relative to σ_{xx} ($T = 2$ K). (Device: B138/C4-1-10 nm Barrier).

though the relative change in resistance appears to be much larger in the hole layer. However, the loss of conductivity in both layers between 2 K and 50 mK (inset Figure 19) is similar (~0.2 mS), over which the insulating behaviour is seen. This is much larger than the change weak localisation (quantum interference) can account for ($\Delta\sigma_{xx} \approx 40\,\mu$S) [75]. Weak localisation predicts that $\Delta\sigma_{xx}(T) = (e^2/2\pi^2\hbar)\ln(\tau_i/\tau_0)$, where τ_i and τ_0 are the temperature-dependent lifetimes for eigenstates of energy and momentum, respectively. The insulating state was also seen in a third device (B141/C5-2) that had been processed with a shorter hall bar (250 μm as opposed to 500 μm), and the effect was found to be independent of the length to width ratio.

Figure 18(e) is an Arrhenius plot ($\ln\rho$ versus $1/T$) for $n = p = 9\times10^{10}$ cm^{-2}, and the resistivity shows a good fit to an activated behaviour (It is difficult to distinguish between a power law and an exponential rise as the insulating phase occurs over a small temperature range, less than one order of magnitude.) ($\rho_{xx}(T) = \rho_0 e^{E/k_BT}$), yielding an energy gap of $E/k_B = 0.4$ K. Similar analysis for the corresponding electron trace (data not shown) gives a far smaller gap of $E/k_B = 0.02$ K. As the density is lowered (Figure 18) and the interaction strength is increased (larger r_s), the fit to an exponential rise becomes poorer. But the traces are expected to be (weakly) insulating for $p < 6\times10^{10}$ cm^{-2}, regardless of the presence of the electrons. The important result is the emergence of a strongly insulating state at *large* $k_F\ell$ ($\rho_{xx} \ll h/e^2$). In Figure 19, $\rho_{xx}(T)$ for both layers appears to saturate at the lowest temperatures. This is likely to an artefact of the electron temperature not reaching the thermometry temperature (Shubnikov-de Haas oscillation amplitude had saturated by ~100 mK, in this measurement run).

7.1. Mismatched Densities. Matching the densities is not crucial to achieving the insulating state. In Figure 21, the hole density was held at $p = 1.6\times10^{11}$ cm^{-2} with the electron density varied ($n = 4, 6, 8\times10^{10}$ cm^{-2}). This was chosen so that for the lowest electron density $n = 4\times10^{10}$ cm^{-2},

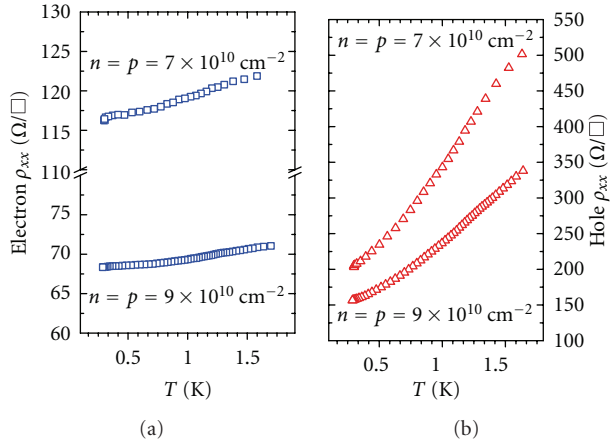

FIGURE 20: Resistivities of hole and electron layers versus temperature for $n = p = 7, 9 \times 10^{10}$ cm^{-2}, with 25 nm $Al_{0.3}Ga_{0.7}$ As barrier. (Device: B135/C3-4-25 nm Barrier).

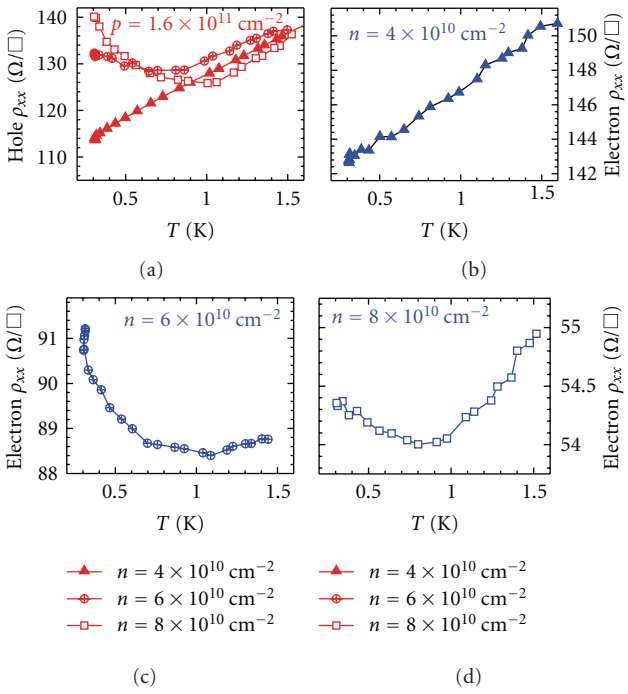

FIGURE 21: Resistivities of the hole (a) and electron layer (b), (c), and (d), versus temperature for fixed hole density $p = 1.6 \times 10^{11}$ cm^{-2}, and varied electron density $n = 4, 6, 8 \times 10^{10}$ cm^{-2}. (Device: B138/C4-1-10 nm Barrier).

both layers have similar resistivities at $T = 1.5$ K. As the electron density is *increased*, both layers undergo a transition from metallic to insulating behaviour. The transition occurs between 4 and 6×10^{10} cm^{-2} when $p \approx 3n$ in this instance, far from matched densities. A transition to insulating behaviour as the density is raised is very striking and incompatible with a disorder-driven mechanism; this strengthens the argument for an interlayer interaction-driven effect.

A similar experiment was performed (down to 50 mK) where n was fixed at 2×10^{10} cm^{-2} and p was varied

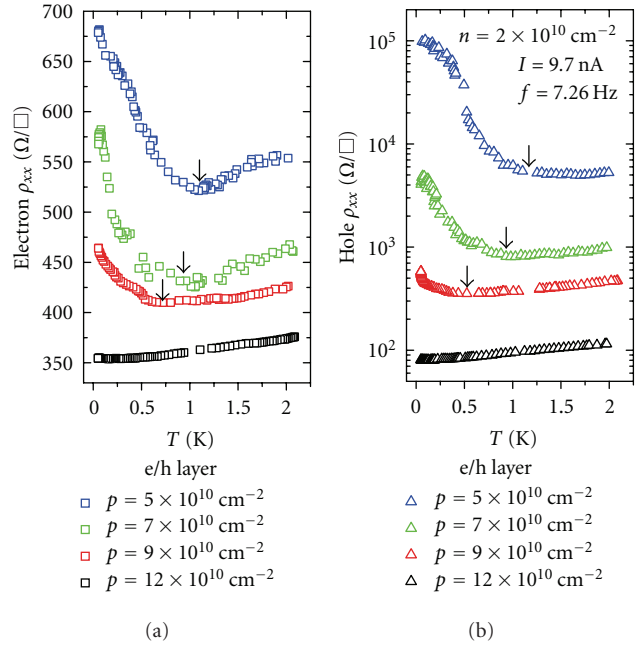

FIGURE 22: Resistivity of electron (a) and hole (b) layers versus temperature, for constant electron density ($n = 2 \times 10^{10}$ cm^{-2}) and different hole densities ($p = 5, 7, 9, 12 \times 10^{10}$ cm^{-2}). Arrows indicate approximate points of transition to insulating behaviour. (Device: B138/C4-2-10 nm Barrier).

(Figure 22). For the largest hole density ($p = 1.2 \times 10^{11}$ cm^{-2}), both layers are metallic, and as the hole density was lowered, both become insulating. Some degree of matching appears to be required for the insulating state to occur, though one would expect that in the limit of p becoming large relative to n (and the hole screening improving accordingly), they would behave as two isolated gases. Arrows in Figure 22 indicate the approximate points of transition to insulating behaviour, suggesting that there may be no abrupt transition as the density is lowered, but a shift in transition temperature.

As the hole density is varied with the electron density held constant ($n = 8.6 \times 10^{10}$ cm^{-2}), $\rho_{xx}(T)$ varies monotonically for both layers across $n = p$ (Figure 23) within the insulating regime at 300 mK. The electron resistance does increase slightly as the hole density is lowered. Matching the densities exactly does not appear to play a significant role. In all the experiments performed, the insulating state appeared to occur in both layers simultaneously, though at higher densities $\rho_{xx}(T)$ has little temperature dependence over the range measured.

7.2. Inhomogeneity. It is important to determine whether the emergent insulating state in the hole layer at large $k_F\ell$ can be attributed to (device-driven) density inhomogeneity. If the hole gas were highly inhomogeneous, the average resistance might be determined by high-density (low-resistance) regions, while the temperature dependence was dominated by low-density insulating regions. It can be established that without the electron gas present, the hole

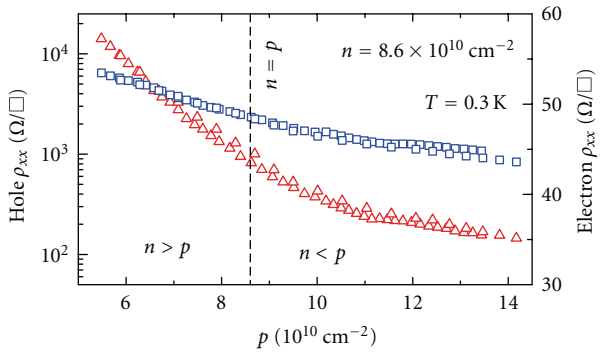

FIGURE 23: Resistivity of electron (blue squares) and hole (red triangles) layers versus hole density, with electron density fixed ($n = 8.6 \times 10^{10}$ cm^{-2}) at $T = 300$ mK. (Device: B138/C4-1-10 nm Barrier).

gas is homogeneous, from the hole layer magnetoresistance (Figure 18). The Shubnikov-de Haas oscillations are periodic in $1/B$ and the reciprocal of the carrier density. A variation in carrier density over the Hall bar region would smear the oscillation. In Figure 18, magnetoresistance traces are shown for four carrier densities, which clearly show well-pronounced oscillations with minima that go to zero for the higher densities. At lower densities, the larger sheet resistance and shorter transport lifetime broaden the Landau levels, requiring lower temperatures for them to be as clearly resolved. Considering only the higher two densities (8 and 9×10^{10} cm^{-2}), the resolution of the oscillations is consistent with the densities measured by the Hall probes at each end of the Hall bar, which record a difference of $\sim 1 \times 10^9$ cm^{-2}.

With the introduction of the electrons, verifying the homogeneity of the 2DHG with magnetoresistance is no longer possible. Indeed, if the insulating state corresponds to a density-modulated phase, then it might be expected that the Shubnikov-de Haas oscillations would no longer be resolved due to the inherent spatial density-variation. Indeed, there are no strong oscillations at 300 mK in the hole layer, but normal oscillations persist in the electron layer at low fields.

If in-built inhomogeneity is the source of the insulating behaviour, it must only be present when the electrons are induced across the barrier. Variation in the thickness of a 10 nm barrier will cause spatial density fluctuations due to a change in interlayer capacitance. MBE growth is capable of producing interfaces that are smooth to a couple of monolayers (0.3 nm for GaAs), giving a possible variation of ~1 nm in the barrier width. This results in a density fluctuation of $\lesssim$10%. (This is an overestimate as the appropriate distance corresponding to the interlayer capacitance is ~25 nm for a 10 nm barrier) and cannot force regions to become insulating ($p < 6 \times 10^{10}$ cm^{-2}) if the average density is 9×10^{10} cm^{-2}. Such inhomogeneity would also be mirrored equally in the electron layer and detectable in the 2DEG magnetoresistance as described above. However, even in the insulating regime the Shubnikov-de Haas oscillations are clearly resolved at 50 mK in the electron layer.

To go from $p, n = 0$ to $n = p$ requires (as well as an increase in interlayer bias) a depleting backgate bias as opposed to an inducing one. It is unclear how backgate action (50 μm away) can produce density variation on the short-length scale required (<60 μm, width of Hall bar/probes). The disagreement in density taken from the Hall slope at each end of the Hall bar is no worse with the electron layer present, (still about 1×10^9 cm^{-2}).

7.3. Two Component Plasma and the Significance of Unequal Electron and Hole Masses. Most of the early theoretical (and numerical) work on the EHBL made the simplifying assumption that the effective masses of the electrons and holes are equal. qSTLS was used by Moudgil et al. 2002 [76] to study the ground state of electron-electron and electron-hole bilayers ($m_e^* = m_h^*$). For the EHBL, a divergence for χ_+ at small q (CDW) was found for $r_s < 10$ with a crossover to the WC state above ($d \sim 4a_B^*$). Unlike [17], a divergence in $\chi_-(q)$ was found for the electron-electron bilayer. They found that the local fields in the electron-electron bilayer are weaker than the EHBL, and the density-modulated phases require larger r_s and smaller d. The results were compared with diffusion Monte Carlo simulations performed on the EHBL by De Palo et al. [65], who were able to show a transition to an excitonic condensate state (BCS-like state) and WC. The WC transition was in good agreement with the qSTLS data. However the CDW state was not considered by De Palo et al. [65].

Subsequent qSTLS work by Moudgil [77] studied the mass-asymmetric EHBL, with $m_h^*/m_e^* = 7$ (appropriate to GaAs) and included the finite widths of the electron and hole gases. The mass-asymmetry pushes the CDW and WC transitions to higher density, though the WC is found to exist only at an intermediate well separation, with the CDW favoured for smaller separations. The larger $r_{s,h}$ in the hole layer is found to be significant, with Wigner crystallisation predicted at $r_{s,e} = 2.4$. Interestingly, the correlation in the hole layer ($g_{hh}(r)$) for the density-modulated phases is found to be *stronger* than in the electron layer ($g_{ee}(r)$). Including a finite QW width was found to lower the critical density for Wigner crystallisation to $r_{s,e} = 3.75$.

More recent work implemented Monte Carlo methods for studying mass-asymmetric EHBLs, with the mass ratio varied [78] between 1 and 100, with the interlayer separation (d) fixed. Electron densities studied corresponded to $r_s \approx 10 - 20$, but for a large layer separation ($d = 20a_B^* \approx 200$ nm in GaAs). They found that by increasing the mass ratio, the hole layer evolves from a homogeneous to a localised state (WC), with the electron layer remaining in a relatively homogeneous state. Periodic structure in $g_{hh}(r)$ exists by $m_h = 5m_e$, a ratio appropriate to GaAs. While these particle densities are considerably lower than those achieved in these experiments, the d/l ratios are similar at ~1.

These results provide a large contrast to the low densities predicted to be required for a WC to occur in a single 2D gas, $r_s = 37 \pm 5$ by Tanatar and Ceperley (1989) [79]. This corresponds to an electron density of $\sim 2 \times 10^8$ cm^{-2}; this is difficult to achieve experimentally in GaAs while maintaining a high mobility such that localisation due to Coulomb

repulsion can be distinguished from that driven by disorder. Hole densities as low as $6 \times 10^8\,\mathrm{cm}^{-2}$ (in GaAs/AlGaAs) have been reported [80], where a much larger r_s is reached (relative to electrons), but at these densities, the 2DHG is in the insulating regime. But in the EHBL, the density-modulated phases are predicted at experimentally accessible r_s that lie within the "metallic" regime.

8. Conclusion

The idea of an excitonic condensate was put forward nearly forty years ago by Blatt et al. [81] and Moskalenko and Snoke [82]. But excitonic phases were initially thought to be necessarily insulating and not accessible by transport because they consisted of charge neutral particles. However, the key experimental development that has radically changed this perspective is the ability to make independent ohmic contacts to the electron-like and the hole-like parts of a system. Experimentally, 2x2DEGs, and 2x2DHGs in a magnetic field have shown striking evidence of transport by neutral objects driven by counterflow currents [33–35]. More recently, electron-hole bilayers in zero magnetic field have shown evidence of an emerging non-Fermi liquid phase [51–53, 70]. In these systems, excitonic phases and collective modes, characteristic of a 2-component plasma, may be competing in determining the ground state. It is very likely that this field will lead to exciting experimental and theoretical results in near future.

Acknowledgments

The work reported here was funded by EPSRC (UK) under the Grants *EP/D008506/1* and *EP/H017720/1*. A. F. Croxall acknowledges Trinity College for a fellowship. I. Farrer acknowledges Toshiba for support. The authors acknowledge several useful discussions with D. Neilson and A. R. Hamilton.

References

[1] Yu. E. Lozovik and V. I. Yudson, "A new mechanism for superconductivity: pairing between spatially separated electrons and holes," *Soviet Physics Journal of Experimental and Theoretical Physics*, vol. 44, p. 389, 1976.

[2] Yu. E. Lozovik and V. I. Yudson, "Feasibility of superfluidity of paired spatially separated electrons and holes; a new superconductivity mechanism," *Journal of Experimental and Theoretical Physics Letters*, vol. 22, p. 274, 1975.

[3] P. J. Price, "Hot electron effects in heterolayers," *Physica B+C*, vol. 117-118, no. 2, pp. 750–752, 1983.

[4] M. B. Pogrebinskii, "Mutual drag of carriers in a semiconductor-insulator-semiconductor system," *Soviet Physics: Semiconductors*, vol. 11, no. 4, pp. 372–376, 1977.

[5] A. P. Jauho and H. Smith, "Coulomb drag between parallel two-dimensional electron systems," *Physical Review B*, vol. 47, no. 8, pp. 4420–4428, 1993.

[6] G. Vignale and A. H. MacDonald, "Drag in paired electron-hole layers," *Physical Review Letters*, vol. 76, no. 15, pp. 2786–2789, 1996.

[7] S. Conti, G. Vignale, and A. H. MacDonald, "Engineering superfluidity in electron-hole double layers," *Physical Review B*, vol. 57, no. 12, pp. R6846–R6849, 1998.

[8] B. Y. K. Hu, "Prospecting for the superfluid transition in electron-hole coupled quantum wells using Coulomb drag," *Physical Review Letters*, vol. 85, no. 4, pp. 820–823, 2000.

[9] A. V. Balatsky, Y. N. Joglekar, and P. B. Littlewood, "Dipolar superfluidity in electron-hole bilayer systems," *Physical Review Letters*, vol. 93, no. 26, Article ID 266801, 2004.

[10] Y. N. Joglekar, A. V. Balatsky, and M. P. Lilly, "Excitonic condensate and quasiparticle transport in electron-hole bilayer systems," *Physical Review B*, vol. 72, no. 20, Article ID 205313, 6 pages, 2005.

[11] P. B. Littlewood and X. Zhu, "Possibilities for exciton condensation in semiconductor quantum-well structures," *Physica Scripta*, vol. T68, p. 56, 1996.

[12] J. Hubbard, "The description of collective motions in terms of many-body perturbation theory II. The correlation energy of a free electron gas," *Proceedings of the Royal Society of London A*, vol. 243, p. 336, 1958.

[13] K. S. Singwi, M. P. Tosi, R. H. Land, and A. Sjölander, "Electron correlations at metallic densities," *Physical Review*, vol. 176, no. 2, pp. 589–599, 1968.

[14] K. S. Singwi and M. P. Tosi, "Correlations in electron liquids," in *Solid State Physics: Advances in Research and Applications*, H. Ehrenreich, Ed., vol. 36, pp. 177–266, Academic Press, New York, NY, USA, 1981.

[15] L. Zheng and A. H. MacDonald, "Correlation in double-layer two-dimensional electron-gas systems: Singwi-Tosi-Land-Sjölander theory at B=0," *Physical Review B*, vol. 49, no. 8, pp. 5522–5530, 1994.

[16] L. Świerkowski, J. Szymański, and Z. W. Gortel, "Coupled electron-hole transport: beyond the mean field approximation," *Physical Review Letters*, vol. 74, no. 16, pp. 3245–3248, 1995.

[17] L. Liu, L. Świerkowski, D. Neilson, and J. Szymański, "Static and dynamic properties of coupled electron-electron and electron-hole layers," *Physical Review B*, vol. 53, no. 12, pp. 7923–7931, 1996.

[18] L. Liu, L. Świerkowski, and D. Neilson, "Exciton and charge density wave formation in spatially separated electron - Hole liquids," *Physica B*, vol. 249–251, pp. 594–597, 1998.

[19] U. Sivan, P. M. Solomon, and H. Shtrikman, "Coupled electron-hole transport," *Physical Review Letters*, vol. 68, no. 8, pp. 1196–1199, 1992.

[20] B. E. Kane, J. P. Eisenstein, W. Wegscheider, L. N. Pfeiffer, and K. W. West, "Separately contacted electron-hole double layer in a GaAs/Al_xGa_{1-x}As heterostructure," *Applied Physics Letters*, vol. 65, no. 25, pp. 3266–3268, 1994.

[21] H. Rubel, A. Fischer, W. Dietsche, K. von Klitzing, and K. Eberl, "Fabrication of indepedently contacted and tuneable 2D electron-hole systems in GaAs-AlGaAs double quantum wells," *Materials Science and Engineering B*, vol. 51, p. 205, 1998.

[22] M. Pohlt, M. Lynass, J. G. S. Lok et al., "Closely spaced and separately contacted two-dimensional electron and hole gases by in situ focused-ion implantation," *Applied Physics Letters*, vol. 80, no. 12, p. 2105, 2002.

[23] J. A. Keogh, K. Das Gupta, H. E. Beere, D. A. Ritchie, and M. Pepper, "Fabrication of closely spaced, independently contacted electron-hole bilayers in GaAs-AlGaAs heterostructures," *Applied Physics Letters*, vol. 87, no. 20, Article ID 202104, 3 pages, 2005.

[24] J. A. Seamons, D. R. Tibbetts, J. L. Reno, and M. P. Lilly, "Undoped electron-hole bilayers in a GaAs/AlGaAs double quantum well," *Applied Physics Letters*, vol. 90, no. 5, Article ID 052103, 2007.

[25] J. P. Eisenstein, L. N. Pfieffer, and K. W. West, "Independently contacted 2-dimensional electron systems in double quantum wells," *Applied Physics Letters*, vol. 57, p. 2324, 1990.

[26] A. F. Croxall, K. Das Gupta, C. A. Nicoll et al., "Patterned backgating using single-sided mask aligners: application to density-matched electron-hole bilayers," *Journal of Applied Physics*, vol. 104, no. 11, Article ID 113715, 2008.

[27] M. V. Weckwerth, J. A. Simmons, N. E. Harff et al., "Epoxy bond and stop-etch (EBASE) technique enabling backside processing of (AI)GaAs heterostructures," *Superlattices and Microstructures*, vol. 20, no. 4, pp. 561–567, 1996.

[28] N. P. R. Hill, J. T. Nicholls, E. H. Linfield et al., "Correlation effects on the coupled plasmon modes of a double quantum well," *Physical Review Letters*, vol. 78, no. 11, pp. 2204–2207, 1997.

[29] M. Prunnila, S. J. Laakso, J. M. Kivioja, and J. Ahopelto, "Electrons and holes in Si quantum well: a room-temperature transport and drag resistance study," *Applied Physics Letters*, vol. 93, no. 11, Article ID 112113, 2008.

[30] K. Takashina, K. Nishiguchi, Y. Ono et al., "Electrons and holes in a 40 nm thick silicon slab at cryogenic temperatures," *Applied Physics Letters*, vol. 94, no. 14, Article ID 142104, 2009.

[31] I. Farrer, A. F. Croxall, K. D. Gupta et al., "MBE growth and patterned backgating of electron-hole bilayer structures," *Journal of Crystal Growth*, vol. 311, no. 7, pp. 1988–1993, 2009.

[32] J. P. Eisenstein and A. H. MacDonald, "Bose-Einstein condensation of excitons in bilayer electron systems," *Nature*, vol. 432, no. 7018, pp. 691–694, 2004.

[33] M. Kellogg, J. P. Eisenstein, L. N. Pfeiffer, and K. W. West, "Vanishing hall resistance at high magnetic field in a double-layer two-dimensional electron system," *Physical Review Letters*, vol. 93, no. 3, Article ID 036801, 2004.

[34] L. Tiemann, J. G. S. Lok, W. Dietsche et al., "Exciton condensate at a total filling factor of one in Corbino two-dimensional electron bilayers," *Physical Review B*, vol. 77, no. 3, Article ID 033306, 2008.

[35] E. Tutuc, M. Shayegan, and D. A. Huse, "Counterflow measurements in strongly correlated GaAs hole bilayers: evidence for electron-hole pairing," *Physical Review Letters*, vol. 93, no. 3, Article ID 036802, 2004.

[36] T. J. Gramila, J. P. Eisenstein, A. H. MacDonald, L. N. Pfeiffer, and K. W. West, "Mutual friction between parallel two-dimensional electron systems," *Physical Review Letters*, vol. 66, no. 9, pp. 1216–1219, 1991.

[37] M. C. Bønsager, K. Flensberg, B. Y. K. Hu, and A. H. MacDonald, "Frictional drag between quantum wells mediated by phonon exchange," *Physical Review B*, vol. 57, no. 12, pp. 7085–7102, 1998.

[38] A. Yurtsever, V. Moldoveanu, and B. Tanatar, "Many-body effects in the Coulomb drag between low density electron layers," *Solid State Communications*, vol. 125, no. 11-12, pp. 575–579, 2003.

[39] R. Asgari, B. Tanatar, and B. Davoudi, "Comparative study of screened interlayer interactions in the Coulomb drag effect in bilayer electron systems," *Physical Review B*, vol. 77, no. 11, Article ID 115301, 2008.

[40] S. Das Sarma and E. H. Hwang, "In-plane magnetodrag in dilute bilayer two-dimensional systems: a Fermi-liquid theory," *Physical Review B*, vol. 71, no. 19, Article ID 195322, 5 pages, 2005.

[41] E. H. Hwang and S. Das Sarma, "Transport and drag in undoped electron-hole bilayers," *Physical Review B*, vol. 78, no. 7, Article ID 075430, 2008.

[42] F. Stern, "Polarizability of a two-dimensional electron gas," *Physical Review Letters*, vol. 18, no. 14, pp. 546–548, 1967.

[43] L. Świerkowski, J. Szymański, and Z. W. Gortel, "Linear-response theory for multicomponent fermion systems and its application to transresistance in two-layer semiconductor structures," *Physical Review B*, vol. 55, no. 4, pp. 2280–2292, 1997.

[44] S. Das Sarma and A. Madhukar, "Collective modes of spatially separated, two-component, two-dimensional plasma in solids," *Physical Review B*, vol. 23, no. 2, pp. 805–815, 1981.

[45] B. Y. K. Hu and J. W. Wilkins, "Two-stream instabilities in solid-state plasmas caused by conventional and unconventional mechanisms," *Physical Review B*, vol. 43, no. 17, pp. 14009–14029, 1991.

[46] M. Kellogg, J. P. Eisenstein, L. N. Pfeiffer, and K. W. West, "Evidence for 2k electron-electron scattering processes in Coulomb drag," *Solid State Communications*, vol. 123, no. 12, pp. 515–519, 2002.

[47] E. H. Hwang, S. Das Sarma, V. Braude, and A. Stern, "Frictional drag in dilute bilayer 2D hole systems," *Physical Review Letters*, vol. 90, no. 8, Article ID 086801, 4 pages, 2003.

[48] R. Pillarisetty, H. Noh, D. C. Tsui, E. P. De Poortere, E. Tutuc, and M. Shayegan, "Frictional drag between two dilute two-dimensional hole layers," *Physical Review Letters*, vol. 89, no. 1, Article ID 016805, 2002.

[49] C. Hodges, H. Smith, and J. W. Wilkins, "Effect of fermi surface geometry on electron-electron scattering," *Physical Review B*, vol. 4, no. 2, pp. 302–311, 1971.

[50] L. Zheng and A. H. MacDonald, "Coulomb drag between disordered two-dimensional electron-gas layers," *Physical Review B*, vol. 48, no. 11, pp. 8203–8209, 1993.

[51] J. A. Seamons, C. P. Morath, J. L. Reno, and M. P. Lilly, "Coulomb drag in the exciton regime in electron-hole bilayers," *Physical Review Letters*, vol. 102, no. 2, Article ID 026804, 2009.

[52] C. P. Morath, J. A. Seamons, J. L. Reno, and M. P. Lilly, "Density imbalance effect on the Coulomb drag upturn in an undoped electron-hole bilayer," *Physical Review B*, vol. 79, no. 4, Article ID 041305, 2009.

[53] A. F. Croxall, K. Das Gupta, C. A. Nicoll et al., "Anomalous coulomb drag in electron-hole bilayers," *Physical Review Letters*, vol. 101, no. 24, Article ID 246801, 2008.

[54] H. B. G. Casimir, "On Onsager's principle of microscopic reversibility," *Reviews of Modern Physics*, vol. 17, no. 2-3, pp. 343–350, 1945.

[55] J. Szymański, L. Wierkowski, and D. Neilson, "Correlations in coupled layers of electrons and holes," *Physical Review B*, vol. 50, no. 15, pp. 11002–11007, 1994.

[56] M. J. Kellogg, *Evidence for excitonic superfluidity in a two dimensional electron system*, Ph.D. thesis, California Institute of Technology, 2005.

[57] C. P. Morath, J. A. Seamons, J. L. Reno, and M. P. Lilly, "Layer interdependence of transport in an undoped electron-hole bilayer," *Physical Review B*, vol. 78, no. 11, Article ID 115318, 2008.

[58] A. Levchenko and A. Kamenev, "Coulomb drag at zero temperature," *Physical Review Letters*, vol. 100, no. 2, Article ID 026805, 2008.

[59] M. P. Lilly, J. P. Eisenstein, L. N. Pfeiffer, and K. W. West, "Coulomb drag in the extreme quantum limit," *Physical Review Letters*, vol. 80, no. 8, pp. 1714–1717, 1998.

[60] X. G. Feng, S. Zelakiewicz, H. Noh et al., "Negative electron drag and holelike behavior in the integer quantum hall regime," *Physical Review Letters*, vol. 81, no. 15, pp. 3219–3222, 1998.

[61] N. P. R. Hill, J. T. Nicholls, E. H. Linfield et al., "Electron-electron scattering between closely spaced two-dimensional electron gases," *Physica B*, vol. 249–251, pp. 868–872, 1998.

[62] J. G. S. Lok, S. Kraus, M. Pohlt et al., "Spin effects in the magnetodrag between double quantum wells," *Physical Review B*, vol. 63, no. 4, Article ID 041305, 4 pages, 2001.

[63] K. Muraki, J. G. S. Lok, S. Kraus et al., "Coulomb drag as a probe of the nature of compressible states in a magnetic field," *Physical Review Letters*, vol. 92, no. 24, Article ID 246801, 2004.

[64] A. Alkauskas, K. Flensberg, B. Y. K. Hu, and A. P. Jauho, "Sign reversal of drag in bilayer systems with in-plane periodic potential modulation," *Physical Review B*, vol. 66, no. 20, Article ID 201304, 2002.

[65] S. De Palo, F. Rapisarda, and G. Senatore, "Excitonic condensation in a symmetric electron-hole bilayer," *Physical Review Letters*, vol. 88, no. 20, Article ID 206401, 4 pages, 2002.

[66] L. Onsager, "Reciprocal relations in irreversible processes. I," *Physical Review*, vol. 37, no. 4, pp. 405–426, 1931.

[67] L. Onsager, "Reciprocal relations in irreversible processes. II," *Physical Review*, vol. 38, no. 12, pp. 2265–2279, 1931.

[68] A. P. Mills Jr., A. P. Ramirez, L. N. Pfeiffer, and K. W. West, "Nonmonotonic temperature-dependent resistance in low density 2D hole gases," *Physical Review Letters*, vol. 83, no. 14, pp. 2805–2808, 1999.

[69] S. Das Sarma and E. H. Hwang, "Calculated temperature-dependent resistance in low-density two-dimensional hole gases in GaAs heterostructures," *Physical Review B*, vol. 61, no. 12, pp. R7838–R7841, 2000.

[70] A. F. Croxall, K. Das Gupta, C. A. Nicoll et al., "Possible effect of collective modes in zero magnetic field transport in an electron-hole bilayer," *Physical Review B*, vol. 80, no. 12, Article ID 125323, 2009.

[71] A. F. Croxall, K. Das Gupta, C. A. Nicoll et al., "Towards the ground state of an electron-hole bilayer," *Physica E*, vol. 42, no. 4, pp. 1247–1250, 2010.

[72] J. Huang, D. S. Novikov, D. C. Tsui, L. N. Pfieffer, and K. W. West, "Interaction effects in the transport of two dimensional holes in GaAs," http://arxiv.org/abs/cond-mat/0610320.

[73] L. H. Ho, W. R. Clarke, A. P. Micolich et al., "Effect of screening long-range Coulomb interactions on the metallic behavior in two-dimensional hole systems," *Physical Review B*, vol. 77, no. 20, Article ID 201402, 2008.

[74] L. Świerkowski, J. Szymański, and Z. W. Gortel, "Intrinsic limits on carrier mobilities in double-layer systems," *Journal of Physics Condensed Matter*, vol. 8, no. 18, pp. L295–L300, 1996.

[75] G. Bergman, "Weak Localisation in thin films: a time of flight experiment with conduction electrons," *Physics Reports*, vol. 107, no. 1, pp. 1–58, 1984.

[76] R. K. Moudgil, G. Senatore, and L. K. Saini, "Dynamic correlations in symmetric electron-electron and electron-hole bilayers," *Physical Review B*, vol. 66, no. 20, Article ID 205316, 10 pages, 2002.

[77] R. K. Moudgil, "Coupled electron-hole quantum well structure: mass asymmetry and finite width effects," *Journal of Physics Condensed Matter*, vol. 18, no. 4, pp. 1285–1301, 2006.

[78] P. Ludwig, A. Filinov, YU. E. Lozovik, H. Stolz, and M. Bonitz, "Crystallization in mass-asymmetric electron-hole bilayers," *Contributions to Plasma Physics*, vol. 47, no. 4-5, pp. 335–344, 2007.

[79] B. Tanatar and D. M. Ceperley, "Ground state of the two-dimensional electron gas," *Physical Review B*, vol. 39, no. 8, pp. 5005–5016, 1989.

[80] J. Huang, D. S. Novikov, D. C. Tsui, L. N. Pfeiffer, and K. W. West, "Nonactivated transport of strongly interacting two-dimensional holes in GaAs," *Physical Review B*, vol. 74, no. 20, Article ID 201302, 2006.

[81] J. M. Blatt, K. W. Böer, and W. Brandt, "Bose-einstein condensation of excitons," *Physical Review*, vol. 126, no. 5, pp. 1691–1692, 1962.

[82] S. A. Moskalenko and D. W. Snoke, *Bose-Einstein Condensation of Excitons and Biexcitons and Coherent Nonlinear Optics with Excitons*, Cambridge University Press, Cambridge, UK, 2000.